Review Article

Carbon Dioxide Corrosion Mechanisms: Historical Development and Key Parameters of CO_2-H_2O Systems

D. Fonseca [ID],[1] M. R. Tagliari [ID],[1] W. C. Guaglianoni [ID],[1] S. M. Tamborim [ID],[1,2] and M. F. Borges [ID][1]

[1]*Physical Metallurgy Laboratory (LAMEF), PPGE3M, Federal University of Rio Grande do Sul (UFRGS), Bento Gonçalves Avenue, 9500, 91501.970 Porto Alegre, Brazil*
[2]*Graduate Program in Chemistry (PPGQ), Federal University of Rio Grande do Sul (UFRGS), Bento Gonçalves Avenue, 9500, 91501.970 Porto Alegre, Brazil*

Correspondence should be addressed to S. M. Tamborim; silvia.tamborim@gmail.com

The recent failures in flexible pipes have motivated the exhaustive research of corrosion mechanisms on high-strength carbon steel armor wires that are the main structural compounds of those structures that mostly operate in seawater environments in the presence of carbon dioxide (CO_2) and confined spaces. Recently, the literature reported discoveries about electrolyte properties (as $Fe^{+2}_{(aq)}$/$HCO_3^-_{(aq.)}$ ratio) and supersaturation, near neutral pH inside the confined space, multiphase reactions of contaminants present in CO_2 gas, the formation and dissolution mechanism of $FeCO_3$ film, and interaction of CO_2 gas impurities with the corrosion scale. Therefore, this review is aimed at presenting an up-to-date narrative of the CO_2 corrosion phenomenon in carbon steel, connecting background fundamentals with current data studies.

1. Introduction

Corrosion drastically impacts the financial costs of the oil and gas industry. The International Measures of Prevention, Application, and Economics of Corrosion Technologies (IMPACT) study, conducted by NACE International, estimates that the global cost of corrosion is about US$2.5 trillion, corresponding to 3.4% of the global gross domestic product (GDP) [1]. The reduced service life of structures, due to the operation in severe service environments, demands investments in maintenance and replacement of components to avoid failures and potential environmental outcomes. Scientists have been investigating ways to overcome or minimize the corrosion issue since it is imperative to guarantee the integrity of the oil and gas equipment.

The discussion concerning CO_2 corrosion, or sweet corrosion, mechanisms in carbon steels was introduced by De Waard and Milliams in 1975 [2] and extends it up to the present day without a definitive conclusion for more varied and complex systems composed of water, carbon steels, and CO_2 [3–6]. In offshore structures, it is common to find CO_2-H_2O environments, such as the annulus space of flexible pipes, where metallic tensile and pressure armors are present. The geological structure where oil and gas are extracted produces different amounts of molecules with corrosive properties (such as water and gases). One of the main corrosive gases in the hydrocarbon product fluids is carbon dioxide (CO_2). When dissolved into the aqueous phase, CO_2 can cause several corrosion processes during transportation from upstream to downstream applications, impacting the inner walls of the rigid carbon steel pipelines [7–9].

Some specific concerns regarding the structure of flexible pipes and operational conditions should be considered when assessing CO_2 corrosion of their armoring steels. Flexible pipe design comprises concentric and nonadherent metallic and polymeric layers responsible for providing radial and axial strength to the structure and barrier protection, respectively. The space between the inner and outer polymeric
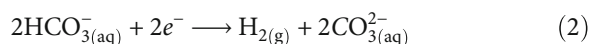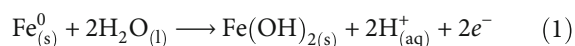
barrier layers, called annulus space, can be flooded with seawater during operation, leading to the corrosion of the metallic armor. The permeation of species such as gaseous CO_2 from production fluids to the annulus throughout the polymeric barrier layers makes the corrosion more severe [8, 10].

External factors such as hydrostatic pressure and annulus properties such as temperature, pH, fugacity of dissolved species, and oxygen presence can influence the resulting corrosion mechanism of carbon steels in such environments [11–14]. Some flexible pipe failure cases related to stress corrosion cracking (SCC) mechanisms in high-content CO_2 gas injection pipes were reported recently in presalt fields. These failures occurred in structures that operated just 10% of their designed life [15], generating an alert about this degradation phenomenon caused by CO_2 and stimulating studies by several research laboratories. This review is aimed at mapping the main contributions of the scientific community over the last 2 decades on CO_2 corrosion mechanisms in carbon steels and discussing the main parameters that influence the severity of corrosion due to CO_2 presence in confined spaces.

2. Fundamentals of the Corrosion Mechanisms in CO_2:H_2O:Steel Systems

The major corrosive agents in the oil and gas industry are carbon dioxide (CO_2), hydrogen sulfide (H_2S), and free water. Corrosion that occurs in environments containing even traces of H_2S is called sour corrosion, while in the presence of CO_2 only, it is denominated sweet corrosion. Nešić [3] published a review about the internal sweet corrosion of carbon steel pipes. Some of the critical factors will be discussed here in the present review, for instance, the electrochemical reactions: (1) the anodic reaction of iron in an aqueous solution and (2) the reduction of bicarbonate ions due to CO_2 corrosion. It is consensus in the literature that reactions (1) and (2) lead to the formation of $FeCO_{3(s)}$ and $H_{2(g)}$ as products of the corrosive phenomenon [2–7, 9, 11–13]. According to Nešić [3], during iron corrosion in an aqueous solution, dissolved CO_2 increases the iron dissolution rate due to the increase in hydrogen evolution reaction.

Regarding the anodic reactions, Nešić [3] agreed with the proposed model by Bockris and Koch [16], which states that the anodic reaction of iron depends on pH. However, the authors showed that this dependency decreases for pH higher than 4. Reactions (1) and (2) are involved in the mechanism proposed by Bockris and Koch [16], Lorenz and Heusler [17], and Moiseeva and Kuksina [18].
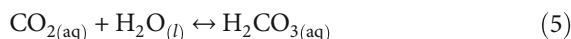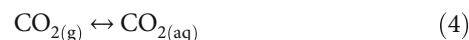
$$Fe^0_{(s)} + 2H_2O_{(l)} \longrightarrow Fe(OH)_{2(s)} + 2H^+_{(aq)} + 2e^- \qquad (1)$$

$$2HCO^-_{3(aq)} + 2e^- \longrightarrow H_{2(g)} + 2CO^{2-}_{3(aq)} \qquad (2)$$

Due to the instability of Fe $(HCO_3)_2$, which forms according to reaction (3), this product dissolves into more ferrous ($Fe^{+2}_{(aq)}$) and bicarbonate ($HCO_3^{-2}_{(aq)}$) ions to the electrolyte.

$$Fe^0_{(s)} + 2\,H_2CO_{3(aq.)} \leftrightarrow Fe(HCO_3)_{2(aq.)} + H_{2(g)} \qquad (3)$$
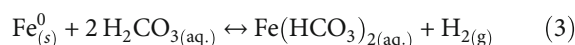
Gray et al. [19] suggested that the direct reduction of bicarbonate ions occurs for CO_2 corrosion at pH <5, according to reaction (2). The corrosion rate decreases with increasing pH at a pH range from 4 to 7.

The study of George and Nešić [20] shows that CO_2 dissolves to produce carbonic acid according to reactions (4) and (5). The first carbonic acid dissociation results in a bicarbonate ion and generates a hydrogen proton (reaction (6)).

$$CO_{2(g)} \leftrightarrow CO_{2(aq)} \qquad (4)$$

$$CO_{2(aq)} + H_2O_{(l)} \leftrightarrow H_2CO_{3(aq)} \qquad (5)$$

$$H_2CO_{3(aq)} \leftrightarrow H^+_{(aq)} + HCO^-_{3(aq)} \qquad (6)$$

In the subsequent dissociation, carbonate ions are formed at a higher pH. The electrons involved in reaction (2) are supplied by the iron dissolution reaction (1). However, it is still a matter of discussion whether carbonic acid diffuses to the metal surface to reduce or acts as a supplier of hydrogen ions through dissociation, being the fastest step. From George and Nešić [20], it is currently accepted that carbonic acid direct reduction reaction (2) is predominant at high CO_2 partial pressures (pCO_2) and high pH values. In contrast, hydrogen reduction becomes predominant for low pCO_2 and pH. Linter and Burstein [21], Moiseeva and Kuksina [18], and Hernandez et al. [22] have proposed a mechanism in two steps. Mora-Mendoza and Turgoose [23] combined these two reactions in order to support their experimental results. Therefore, at pH 3.8, the concentration of bicarbonate ions is low, then the precipitation is given in the following:

$$Fe^{2+}_{(aq)} + HCO^-_{3(aq)} \leftrightarrow FeCO_{3(aq)} + H^+_{(aq)} \qquad (7)$$

As stated by Hernandez et al. [22] and Sun et al. [24], the process of mass transport when CO_2 is in contact with water can be explained by the formation of $FeCO_3$, including the local acidification process that will dissolve $FeCO_3$ and result in porous scales.

Tran et al. [25] elucidated the mechanism of CO_2 corrosion, through either the direct reduction of bicarbonate or the buffer effect by supplying $H^+_{(aq.)}$ ions and catalyzing the hydrogen reduction reaction. The build-up of hydrogen ions in solution promotes its reduction on the metal surface.

Considering the buffer effect, Tran et al. [25] questioned whether only the thermodynamically based arguments of Linter and Burstein [21] are sufficient to prove that the reduction of carbonic acid cannot be considered a contributor to hydrogen ions. The authors concluded that the corrosion rate is proportional to the partial pressure of CO_2 because they related the reduction of carbonic acid as the dominant mechanism. Nevertheless, if the dominant mechanism is the buffer effect with the predominant cathodic reaction, the corrosion rate will increase due to the increase

in pCO_2 only when the corrosive process is controlled by mass transport.

Tran et al. [25] showed that when the concentration of hydrogen ions increases (i.e., the pH decreases), the charge transfer current increases, regardless of the presence of CO_2 or not. As well as for different pCO_2 (1 and 10 bar), the variation of pH and temperature parameters did not change their respective charge transfer currents, confirming that hydrogen ions will permanently be reduced. The authors concluded that the predominant mechanism is the buffer effect under the conditions in which the authors performed their experiments. The predominant reaction is the reduction of hydrogen ions, with carbonic acid being relevant only to act as a source of hydrogen ions due to its dissociation. The compounds arising from the CO_2 hydration process are directly linked to the increase in the iron dissolution rate.

Regarding CO_2 corrosion mechanisms in mild steel, Kahyarian et al. [26] investigated the preponderance of buffer effects and direct reduction of carbonic acid. They found that the direct reduction of carbonic acid is irrelevant, similar to Tran et al. [25]. On the other hand, the increase of carbonic acid concentration in the system, due to the increase of pCO_2, also increases the cathodic current limit because the hydration restores the concentration of carbonic acid, supplying hydrogen ions for later reduction at the metallic surface. The kinetics of iron dissolution, when exposed to CO_2, suggests a relationship between CO_2 or its corresponding species and the corrosion of iron, which goes against what was predicted by Bockris et al. [27]. Finally, carbon steel, when immersed in an acid solution in the presence of CO_2, promotes the increase in the corrosion rate of steel due to the ability to buffer CO_2 and carbonic acid, producing an increase in the cathodic current limit [27]. A deeper investigation of the chemistry related to the solution test or seawater employed in the corrosion tests should be necessary.

Typically, sweet corrosion occurs when H_2O in a vapor or liquid state is unsaturated, saturated, or supersaturated by CO_2 molecules, or it occurs when gaseous or supercritical CO_2 is unsaturated, saturated, or supersaturated by water molecules [28–30]. CO_2 corrosion in H_2O (unsaturated or saturated with CO_2) involves a phenomenon of $CO_{2(aq.)}$, $HCO_3^{-2}{}_{(aq.)}$, and $CO_3^{-2}{}_{(aq.)}$ dissolution and $FeCO_3$ precipitation (Figure 1). The dissolved salts can modify the phase portioning of H_2O and CO_2 because they can change the solubility. Generally, the corrosion rate is higher at the initial immersion time and becomes lower after long immersion times due to the formation of corrosion products on the steel surface, leading to pseudo passivation of the substrate.

Several authors have observed differences between the corrosion mechanisms for supercritical CO_2, that is, at temperatures and pressures above the critical point (31.1°C and 73.8 bar), with gaseous or liquid CO_2 [28, 31, 32]. The solubility of CO_2 in water increases dramatically from the critical point onwards [29, 30], which directly impacts the concentration of H_2CO_3, HCO_3^-, and CO_3^-. The increase in the concentration of carbonic species accelerates the electrochemical reactions and consequently increases the corrosion rate [33].

2.1. Electrolyte Equilibria.

2.1. Electrolyte Equilibria. The conditions where the steels are exposed, the comprehension of the environment at all, comprising brines, condensed water, gas, or dense phases with their impurities, affect physic-chemical parameters where corrosion takes place, with consequent effect on corrosion mechanisms and severities. In this way, some relevant parameters regarding these will be commented.

Several seawater parameters can be modified with water depth increase, such as salinity, pH, temperature, pressure, and oxygenation grade, depending on the condition of exposure of some equipment. During laboratory corrosion tests, in order to better represent and compare the results, the majority of researches showed here follows the recommendations of ASTM D1141, SSW, or NaCl5% as test environments, as they represent many situations in the O&G industry [19, 34].

According to specific situations of operation, other solutions can be employed, such as those containing distilled water saturated by CO_2 or brines saturated by $CO_{2(g)}$. Some examples of electrolytes employed in the literature can be cited as follows:

(i) NaCl 3.2 mol.L^{-1} with adjusted pH to around 4 with HCl or $NaHCO_3$ (Almeida and Bandeira [12])

(ii) NaCl 0.2 wt% with adjusted pH from 6 to 6.6 with $NaHCO_3$ (De Motte et al. [35])

(iii) NaCl 1 wt% with adjusted pH to around 6 with $NaHCO_3$ (Rizzo et al. [36])

(iv) Distilled water with $CO_{2(g)}$ at saturated (1 or 30 bar of $CO_{2(g)}$) or supercritical conditions (110 bar and 40°C) with adjusted pH to 4 with $NaHCO_3$ (Almeida and Bandeira [12])

(v) Solutions that simulate the soil in conditions close to neutrality, composed of $CaCO_3$, KCl, $MgSO_4$, $CaCl_2$, and $NaHCO_3$ sprinkled with a mixture of gases such as CO_2/N_2 and O_2 [37]

The presence of dissolved salts and weak acids proves that the water chemistry is more complex than pure distilled water or only saturated by $CO_{2(g)}$. The concentration of dissolved salts can be high (>10 wt%), comprising a nonideal solution.

Equation (8) shows the concentration of $CO_{2(g)}$ dissolved in seawater that depends on its salt concentration [38]. This improved model proves that the electrolyte composition has the main role in corrosion behavior. It considers the various salts that can precipitate if their solubility is exceeded, such as $FeCO_3$, $CaCO_3$, and $CaSO_4$ [3, 4, 34].

$$
\begin{aligned}
Ln\, m_{CO_2} = {} & Ln\, \gamma_{CO_2}\varphi_{CO_2}P - \frac{\mu_{CO_2}}{RT} \\
& - 2\sigma_{CO_2-Na}\left(m_{Na} + m_{Ca} + m_K + m_{Mg}\right) \\
& - \delta_{CO_2-Na-Cl}\, m_{Cl}\left(m_{Na} + m_{Ca} + m_K + m_{Mg}\right) \\
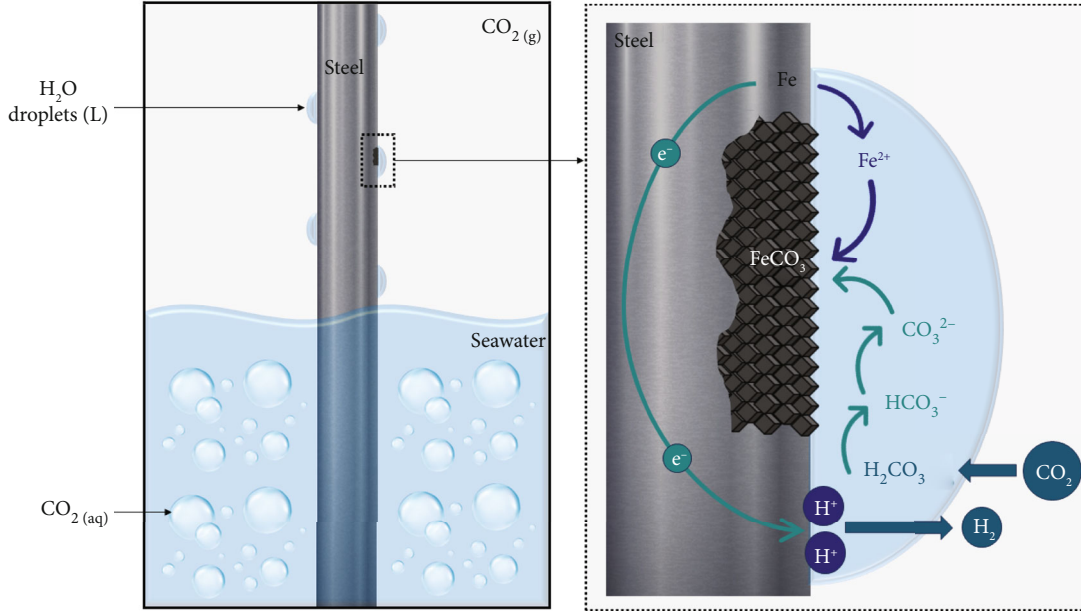& + 0.7\, m_{SO_4},
\end{aligned}
\tag{8}
$$

FIGURE 1: Schematic diagram of CO_2 corrosion in carbon steel.

where γ_{CO_2} is related to the molar fraction of carbon dioxide in the vapor phase, φ_{CO_2} is related to carbon dioxide fugacity, P represents the total pressure of the system, μ_{CO_2} is related to the chemical potential of carbon dioxide at standard conditions (at around -393 kJ/mol), RT is the product between the ideal gas constant (8,134 joule/molK), T is the temperature in kelvin, σ_{CO_2-Na} and $\delta_{CO_2-Na-Cl}$ are related to interaction parameters between carbon dioxide with sodium cation and carbon dioxide with Na-Cl, respectively, m_{Na}, m_{Ca}, m_K, and m_{Mg} are related to the molarity of cations: sodium, calcium, kalium, and magnesium, respectively, m_{Cl} is related to chloride molarity, and m_{SO_4} is related to sulfate molarity.

The dissolved ions in seawater produce the "salting effect," whereas a minor CO_2 amount is dissolved compared to distilled water or water containing minor concentrations of salts. In this sense, the ionic strength (IS) equation shown in (9) can predict the ranking of the salting-out effect [38].

$$IS = \frac{1}{2} \sum_{1}^{n} Z_i m_i, \qquad (9)$$

where Z_i represents the charge of ionic species and m represents the concentration of a solution containing this ion in mol.L^{-1}.

Pressure and temperature can modify the phases in the system $CO_{2(g)}:H_2O_{(l)}$ [39, 40]. Pressure-temperature data for $CO_2(g):H_2O_{(l)}$ system comprises the coexistence of phases, such as
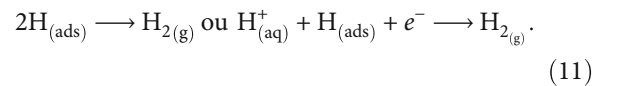
(i) Vapor rich in CO_2 or H_2O

(ii) Liquid rich in CO_2 or H_2O, and

(iii) Hydrates of crystalline substances composed by an open water molecule network arranged to entrap guest molecules

In pure water saturated by CO_2, two quadrupoles can be observed: Q_1 (11.8 bar and -1.43°C) and Q_2 (46 bar and 9.93°C). A recent study by Zadeh et al. [39] is in accordance with Diamond and Akinfiev [40], where four phases in equilibrium are achieved based on phases: L_1 or LCO_2 liquid (liquid richer in CO_2), L_2 or LH_2O (liquid richer in H_2O), vapor richer in $CO_2(g)$, and Cla (identified as CO_2-clathrate hydrate or hydrate) until the lower critical end-point (LCEP).

The chemical equilibrium of seawater components, the physical equilibrium of gaseous components dissolved in seawater, and the impurities present in $CO_{2(g)}$ justify the study of complex mechanisms involving the speciation of dissolved components present in a $CO_{2(g)}:H_2O_{(l)}$ system with pH variation.

2.1.1. pH and Dissolved Species. Many researchers over the years proposed different CO_2 corrosion mechanisms. De Waard and Milliams were the first to propose a mechanism for this system in the '70s [2]. Considering the cathodic reaction as the rate-determining step, a Volmer-Heyrovsky mechanism for cathodic reactions of carbon steel in an acid solution was proposed according to the following reactions:

$$H^+_{(aq)} + e^- \longrightarrow H_{(ads)}, \qquad (10)$$

$$2H_{(ads)} \longrightarrow H_{2(g)} \text{ ou } H^+_{(aq)} + H_{(ads)} + e^- \longrightarrow H_{2(g)}. \qquad (11)$$

Gray et al. [19] correlated the corrosion rates with carbonic acid concentration at different pressures and

temperatures. It could be expressed by equation (12), where i_c is the corrosion current.

$$\log i_c = -A * pH + B. \tag{12}$$

The constant A depicts the dependence of the anodic dissolution on the pH. The more significant value for A, obtained experimentally, suggests a correlation between corrosion rate and the concentration of undissociated carbonic acid, i.e., pH. Given equation (13) and since the concentration of carbonic acid is proportional to the CO_2 partial pressure (pCO$_2$), according to Henry's law, equations (12) and (13)

$$pH = -\frac{1}{2} * \log P_{CO_2} + \text{constant}. \tag{13}$$

Equation (14) could be expressed as

$$\log i_c = \frac{1}{2} * A * \log P_{CO_2} + B'. \tag{14}$$

The referred proposed corrosion mechanism from De Waard and Milliams [2] starts from the already established relationship between potential (E) and current density for anodic dissolution (i_a).

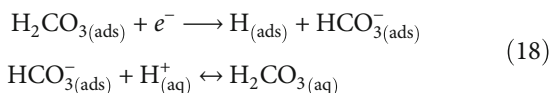$$E = b_a * \log i_a - b_a * pH + c_a. \tag{15}$$

The same can be done for the cathodic current density when it is assumed that reactions (10) and (11) are the cathodic reactions of the system, as follows:

$$E = b_k * \log i_k - b_k * pH + c_k. \tag{16}$$

Alternatively, the authors assumed that there is no diffusion limitation in the range of potentials, therefore eliminating the E potential from equations (15) and (16), reached at (8), with A equal to

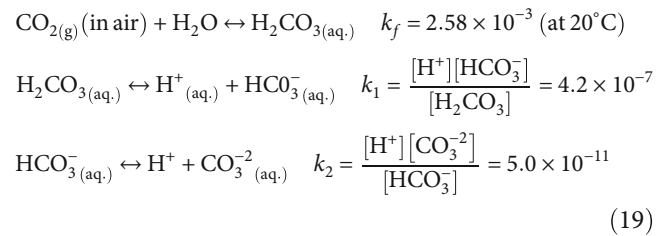$$A = \frac{b_k - b_a}{b_k + b_a}. \tag{17}$$

However, the A values calculated by De Waard and Milliams [2] did not correspond to the experimental value of A equal to 1.3. Assuming 40 mV/dec and 120 mV/dec, the values of the anodic and cathodic Tafel slopes, respectively, the authors reached a value of A equal to 0.5. Therefore, the high A value obtained experimentally suggests a possible correlation of the corrosion rate with the concentration of carbonic acid. Thus, a catalytic mechanism for the cathodic reaction was proposed based on the following reactions:

$$\begin{aligned} &H_2CO_{3(ads)} + e^- \longrightarrow H_{(ads)} + HCO_{3(ads)}^- \\ &HCO_{3(ads)}^- + H_{(aq)}^+ \leftrightarrow H_2CO_{3\,(aq)} \end{aligned} \tag{18}$$

The linear relation between pH and corrosion current of carbon steel associated with CO_2 in pipelines comprises the

empirical/semiempirical models that consider the fundamental physicochemical processes studied in the 1980s and 1990s [19, 34]. The papers assume that carbon dioxide is almost always present as a byproduct of natural gas extraction in this hydrated form (H_2CO_3), and the fundamental physicochemical process underlying uniform CO_2 corrosion is discussed with a mathematical relationship.

The literature proves that all chemical reactions of the CO_2:H_2O system were strongly affected by $H^+_{(aq.)}$ concentration and $CO_{2(g)}$ pressure by the respective relations due to saturation of water with $CO_{2(g)}$ followed by its dissociation steps and correspondent equilibrium constants according to the following equations [22]:

$$CO_{2(g)}(\text{in air}) + H_2O \leftrightarrow H_2CO_{3(aq.)} \quad k_f = 2.58 \times 10^{-3} \text{ (at } 20°C)$$

$$H_2CO_{3(aq.)} \leftrightarrow H^+_{(aq.)} + HCO_{3\,(aq.)}^- \quad k_1 = \frac{[H^+][HCO_3^-]}{[H_2CO_3]} = 4.2 \times 10^{-7}$$

$$HCO_{3\,(aq.)}^- \leftrightarrow H^+ + CO_{3\,(aq.)}^{-2} \quad k_2 = \frac{[H^+]\left[CO_3^{-2}\right]}{[HCO_3^-]} = 5.0 \times 10^{-11}$$

$$\tag{19}$$

The proportional relation between the concentration of carbonic acid $[H_2CO_3]$ and CO_2 partial pressure (P_{CO_2}) (equation (20)) and the relation between the concentration of bicarbonate and carbonate ions with pH and CO_2 pressure (equations (21) and (22), respectively) suggests that the dissociation of H_2CO_3 is followed by the reduction of H_2, evidencing the buffering effect [22, 41].

$$\text{Log}[H_2CO_3] \leftrightarrow -1.43 + P_{CO_2} \tag{20}$$

$$\text{Log}[HCO_3^-] \leftrightarrow -7.8 + \text{Log}\,P_{CO_2} - \text{LogH}^+_{(aq.)} \tag{21}$$

$$\text{Log}\left[CO_3^{-2}\right] \leftrightarrow -18.14 + \text{Log}\,P_{CO_2} - 2\,\text{LogH}^+_{(aq.)} \tag{22}$$

De Waard and Milliams [2] proposed equation (23) to predict the rate and mechanism of carbon dioxide corrosion on carbon steel, which depends on the partial pressure of CO_2 and temperature.

$$\text{Log}\,V_C = 7.96 - \frac{2320}{273.2 + T°} - \frac{5.55}{1000}\,T° + 0.67\,\text{Log}\,p_{co_2}, \tag{23}$$

where V_c is the surface average rate of metal weight loss (g/(m^{2}h)), p_{CO2} is the partial pressure of carbon dioxide (bar), and $T°$ is the temperature (°C) (applicable at pCO$_2$ < 10 bar and T < 140°C).

The pCO$_2$, described by equation (23), presents a strong effect on pH, which is associated with the dissociated species of CO_2 in water (see equations (20)–(22)), as well as adsorbed species [18].

$$\begin{aligned} CO_{2(g)}(\text{in air}) + H_2O &\leftrightarrow CO_{2(\text{soluble})} + H_2O \\ &\leftrightarrow CO_{2(ads)} + H_2O \leftrightarrow H_2CO_{3(ads.)} \end{aligned} \tag{24}$$
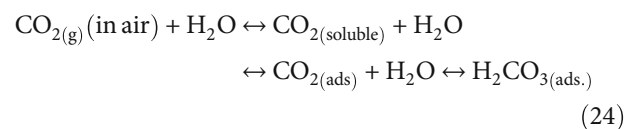
The pH act directly on corrosion behavior as the primary determining factor on the cathodic half-reaction of the corrosive phenomenon of CO_2 of steel alloy, whereas the anodic half-reaction at free oxygen conditions in a wide pH range is the following reaction [18]:

$$Fe^{\circ}{}_{(s)} + 2\,H_2O \leftrightarrow Fe(OH)_{2\,(S)} + 2\,H^+_{(aq.)} + 2e^- \qquad (25)$$
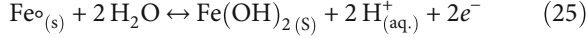
Moiseeva and Kuksina [18] proposed the half-cathodic reactions shown in Table 1, where the reactions are divided according to the pH range, as follows:

(i) pH <5: $CO_{2(g)}$ exists in the molecular form mainly and $H_2CO_{3(ads)}$ is the main depolarizer of the cathodic process according to Table 1

(ii) pH ~6.5 to 6.8: the ratio between H_2CO_3 e HCO_3^- in solution is approximately 3:7, and the cathodic process can be followed in two ways as presented in Table 1

(iii) pH >6.8: the percentage of bicarbonate ions in aqueous solutions achieves 99%. Under those conditions, dissolved bicarbonate ions are the dominant depolarizers according to Table 1. On the other hand, the anodic half-reaction (Table 1) produces a siderite film at pH >6.8. The previous layer of iron hydroxide (Table 1) reacts with bicarbonate anion producing more siderite film (Table 1). The bicarbonate ions in excess can react with iron carbonate promoting the dissolution of siderite film according to Table 1 that shows the complex soluble $[Fe(CO_3)_2]^{-2}{}_{(aq.)}$

(iv) pH ≥7: the cathodic half-reaction dominant is the H_2O reduction that increases OH^- ions in solution (Table 1). CO_3^{2-} ions accumulate in solution according to Table 1

It is crucial to remember that pH acts directly on the corrosive phenomenon but never alone. The temperature can intensify the corrosion phenomenon because it promotes a more porous and permeable corrosion product layer on the steel surface (reactions in Table 1) between 25 and 40°C. A denser layer on the steel surface can modify the corrosion mechanism, promoting a deceleration of the general corrosion at 60°C (according to reactions for pH > 6.8 shown in Table 1) [18] due to pseudopassivation effects.

The reduction reactions of carbonic acid and bicarbonate anion (reactions (26) and (27)), with a decreased proton concentration near to surface (reaction (28) and reduction of water (reaction (29)), promote a higher pH on the surface when compared to the bulk values according to a study carried out with NaCl 1 wt% saturated with $CO_{2(g)}$ [42, 43].
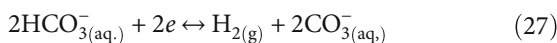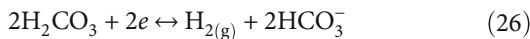
$$2H_2CO_3 + 2e \leftrightarrow H_{2(g)} + 2HCO_3^- \qquad (26)$$

$$2HCO_3^-{}_{(aq.)} + 2e \leftrightarrow H_{2(g)} + 2CO_3^-{}_{(aq.)} \qquad (27)$$

TABLE 1: Half-cathodic reactions according to the pH range for the $CO_{2(g)}$:$H_2O_{(l)}$:steel system [18].

pH range	Half-cathodic reactions
pH <5	$H_2CO_{3\,(ads)} + e \leftrightarrow H^+_{ads.} + HCO_3^-{}_{(ads.)}$
6.5< pH <6.8	$HCO_3^-{}_{(sol.)} + e \leftrightarrow H_{ads.} + CO_3^{2-}{}_{(aq.)}$
	$HCO_3^-{}_{(ads.)} + e \leftrightarrow H_{ads.} + CO_3^{2-}{}_{(aq.)}$
	$2\,H_{ads.} \longrightarrow H_{2\,(ads.)}$
pH >6.8	$HCO_3^-{}_{(sol.)} + Fe^0_{(s)} \leftrightarrow FeCO_{3(s)} + H^+_{(aq)} + 2e$
	$Fe(OH)_{2(s)} + HCO_3^-{}_{(aq.)} \leftrightarrow FeCO_{3(s)} + H_2O_{(l)} + OH^-_{(l)}$
	$FeCO_{3(s)} + HCO_3^-{}_{(aq.)} \leftrightarrow \left[Fe(CO_3)_2\right]^{-2}{}_{(aq.)} + H^+_{(aq.)}$
pH ≥7	$2H_2O + 2e \leftrightarrow H_{2(g)} + 2\,OH^-_{(aq.)}$
	$HCO_3^{2-} + OH^-_{(aq.)} \leftrightarrow CO_3^{2-}{}_{(aq.)} + H_2O$

$$2H^+ + 2e \leftrightarrow H_{2(g)} \qquad (28)$$

$$2H_2O + 2e \leftrightarrow H_{2(g)} + 2\,OH^-_{(aq.)} \qquad (29)$$

A series of measurements were performed by Han et al. [44] to compare bulk pH (pH_{bulk}) to surface pH ($pH_{surface}$) in the corrosive process of mild steel. The corrosion tests employed a NaCl 1 wt% solution (saturated with CO_2) at a total pressure of 1 bar CO_2 and partial pressure of 0.97 CO_2. The authors observed a higher $pH_{surface}$, approximately 5.7 at 25°C and 6.2 at 80°C, while the pH_{bulk} was approximately 4 for the studied temperature range.

The diffusion coefficients of species from the bulk are often a limiting factor because protons are consumed on the steel surface faster. As can be seen in Table 2, $H^+_{(aq.)}$ presents a higher diffusion coefficient ($9.312 \times 10^{-9}\ m^2/s$) when compared to other species involved [45].

The conditions of thermodynamically nonideal solutions, such as seawater, should be preserved as closely as possible in the laboratory corrosion tests to reproduce operational conditions. In this sense, experiments carried out in artificial seawater solution (ASTM D-1141 [49]) prove this similarity at pH 8.2 [3, 50]. This estimation assumed that the infinite dilution theory is valid, i.e., the activity coefficients for all chemical species are assumed to be the unity. The effect of nonideal behavior consists of systems with higher pressures where ion-ion and ion-neutral molecule interactions can be significant, promoting changes in the concentration of solutions and affecting speciation and transport properties, typical for concentrated electrolytes such as seawater [51]. Regarding speciation, the association of ions needs to be considered. The presence of undissociated neutral species promotes significant changes in conductivity, concentration, and activity coefficients in NaCl 0.05 mol.L^{-1} [50].

Seawater saturated with $CO_{2(g)}$ decreases the pH to 5 and strongly influences the corrosion rate, as showed experimentally and computationally by Dugstad [52]. The typical pH of CO_2-saturated condensed water is about 4. Figure 2(a)

TABLE 2: Diffusion coefficients of reacting species from bulk in CO_2:seawater:steel system (adapted from [45–48]).

Species	Diffusion coefficients (m^2/s)	Source
$H^+_{(aq.)}$	9.312×10^{-9}	[35]
$OH^-_{(aq.)}$	5.26×10^9	[36]
$CO_{2(g)}$	1.96×10^{-9}	[35]
$H_2CO_{3(aq.)}$	2.00×10^{-9}	[37]
$HCO_3^-{}_{(aq.)}$	1.105×10^{-9}	[36]
$CO_3^{-2}{}_{(aq.)}$	0.92×10^{-9}	[37]
Cl^-	2.032×10^{-9}	[36]
$Na^+_{(aq.)}$	1.334×10^{-9}	[36]
$Ca^{+2}{}_{(aq.)}$	0.79×10^{-9}	[36]
$Fe^{+2}{}_{(aq.)}$	0.72×10^{-9}	[37]
$Ba^{+2}{}_{(aq.)}$	0.847×10^{-9}	[36]
$Sr^{+2}{}_{(aq.)}$	0.791×10^{-9}	[36]

shows the concentration of $CO_{2(aq.)}$, $H_2CO_{3(aq.)}$, $HCO_3^-{}_{(aq)}$, and $CO_{3(aq)}^{-2}$ in synthetic seawater (SSW) according to the pH values proposed by König et al. [53] and by Kahyarian et al. in 2016 [50], the last in solution 0.5 mol.L^{-1} NaCl (Figure 2(b)). For these two environments, the effect of bicarbonate ions is preponderant when the $CO_{2(g)}$ buffered brine turns the pH value to around 5.

The simulated soil solution used by Wang et al. [37] represents a more conductive environment at near-neutral conditions, similar to the external environment of buried pipelines where near-neutral stress corrosion cracking occurs. This electrolyte is composed by 0.05 mmol.L^{-1} KCl, 0.11 mmol.L^{-1} MgSO$_4$.7H$_2$O, 0.17 mmol.L^{-1} CaCl$_2$.2H$_2$O, 0.23 mmol.L^{-1} NaHCO$_3$, and 0.61 mmol.L^{-1} CaCO$_3$. The solution was bubbled with a gas mixture composed of 5% CO$_2$/balance N$_2$ or 3%O$_2$ and 5% CO$_2$/balance N$_2$.

The pH has a direct effect on the corrosion rate and the direct reduction of $H^+_{(aq)}$ ions for pH ≤4, particularly at a lower partial pressure of CO$_2$ [42]. The probability of involving $H_2CO_{3(aq)}$ and $HCO_3^-{}_{(aq)}$ soluble or adsorbed species and molecular or dissolved species such as $CO_{2(ads.)}$, $CO_{2(sol.)}$, and $CO_3^{2-}{}_{(aq)}$ as depolarizers in oxygen-free aqueous media saturated with CO$_2$ depends on the partial pressure of CO$_2$, pH, temperature, and the hydrodynamic parameters of the environment. So, variations in pH and pCO$_2$ change the pattern of cathodic and anodic processes. The general equation for the cathodic reaction rate can be given by the following equation [50]:

$$i_{\text{cathodic}} = F.k_c.[CO_2] \exp\left[\frac{-\alpha.F.E}{RT}\right], \tag{30}$$

where F is the Faraday constant, k_c is the reaction constant, and $[CO_2]$ is the CO$_2$ concentration in the solution.

Barker et al. [4] showed that pH can act on the CO_2:H_2O equilibrium by significant variations in $Fe^{+2}{}_{(aq.)}$ solubility in

a solution containing chloride ions at different pressures from Dugstad et al.'s [52] study. It is plausible to conclude that differences in pH from the metal surface (pH ~5.7) to bulk (pH ~6.2) provide different quantities of dissolved Fe^{+2} across the solution, i.e., from the metal surface to the bulk electrolyte, resulting in a variation of the amount of FeCO$_3$ that is deposited [44].

The probability of corrosion or precipitation and scaling tendency is related to the speciation chemistry of Fe^{+2} and Fe^{+3} modified according to pH values in seawater (Figure 3). As the Fe^{+2} (Figure 3(a)) concentration decreases for pH greater than 8 and the Fe^{+3} (Figure 3(b)) concentration decreases for pH greater than 4.5, the iron dissolved concentration in seawater is minor: around 0.05 to 2 n.mol.L^{-1} [54]. In the same way, the precipitation of ferrous compounds, such as FeCO$_3$, occurs under specific conditions of pH, temperature, and strength force according to previous works [55].

The possibilities of corrosion or precipitation rate and scaling tendency according to pH values were reported by Nešić et al. [42], and all possibilities are the results of the complex mechanism of saturation, nucleation by precipitation, and growth of siderite film. This mechanism is a consequence not only of the pH values but also of temperature and pressure effects. Hence, the equations explained in this chapter should be associated with dissolved iron and supersaturation to better clarify the sweet corrosion.

2.1.2. Dissolved Iron and Corrosion Rate. Carbon steels are employed in several offshore components that face CO$_2$ corrosion. The major microstructures present in these steels are composed of ferrite and perlite, and when exposed to environments containing water and CO$_2$, preferential ferrite dissolution occurs, leaving the lamellar cementite (Fe$_3$C), which is a more noble structure on the surface [56, 57]. Cementite acts as a cathode, and hydrogen reduction occurs on this structure, creating a galvanic coupling with ferrite and accelerating the ferrite dissolution, which contributes to iron dissolved as a contaminant in seawater. The preferred dissolution of ferrite also contributes to the localized corrosion process, besides other factors such as alloy composition, heat treatment, surface defects, level and nature of nonmetallic inclusions, and slip band dissolution [58, 59]. For closed systems, such as flexible pipe annulus, $Fe^{+2}{}_{(aq)}$ was indicated as a contaminant and is found soluble in a very small volume, turning the flooded annulus region supersaturated with iron [60, 61].

The carbonic gas dissolved in seawater can act like chemical binders and catalyze iron dissolution, independent of pH [62]. This behavior can increase iron anodic dissolution without iron carbonate protection according to reaction (31). Whereas Linter and Burstein [21] proposed that the kinetic of iron dissolution is not affected by CO$_2$, independent of the corrosion mechanism, the opposite was proposed by Nešić et al. [63].

$$Fe_{(s)} \longrightarrow Fe^{2+}_{(aq)} + 2e^- \tag{31}$$
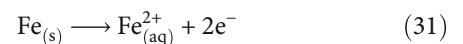
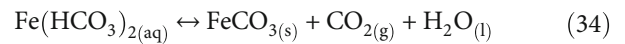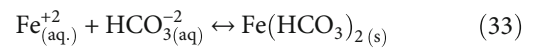Then, carbon steel corrodes in environments containing CO$_2$, producing dissolved iron in seawater, which can react
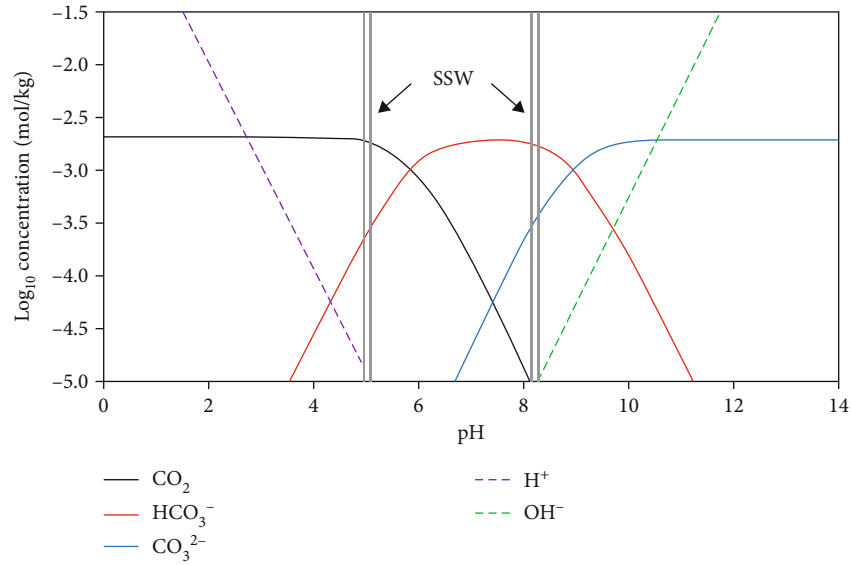
(a)
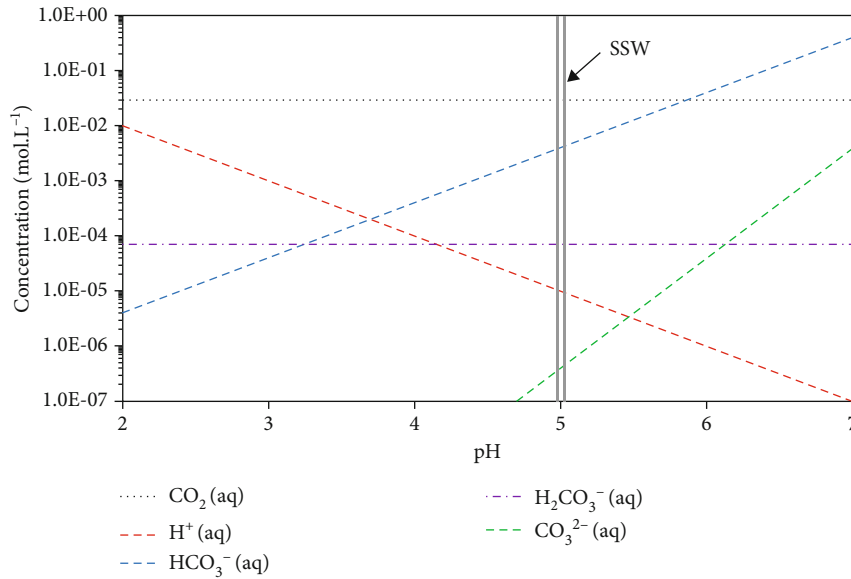
(b)

Figure 2: Concentration of chemical species dissolved in the carbonate/seawater system (a) $CO_{2(aq)}$ black line, $HCO_{3(aq)}^-$ red line, $CO_{3(aq)}^{-2}$ blue line, $H^+_{(aq)}$ dotted black line, and $OH^-_{(aq)}$ dotted red line (reproduced from König et al. [53] under the Creative Commons Attribution License/public domain) and (b) $CO_{2(aq)}$ doted black line, $H^+_{(aq)}$ doted red line, $HCO_{3(aq)}^-$ dotted blue line, $H_2CO_{3(aq)}$ dotted gray line, and $CO_{3(aq)}^{-2}$ dotted blue line in CO_2/water equilibrium at $pCO_2 = 1$ bar, $T = 25°C$, and 0.5 M NaCl (reproduced from Kahyarian et al. [50] under the Creative Commons Attribution License/public domain).

with carbonate anions and produce a corrosion film composed mainly of iron carbonate or siderite ($FeCO_3$) (reaction (32)). Thus, $FeCO_3$ is believed to occur through a one-step reaction process with carbonates. However, a two-step reaction involving bicarbonates (reactions (33) and (34)) has also been proposed [4].

$$Fe^{+2}_{(aq)} + CO^{-2}_{3(aq.)} \leftrightarrow FeCO_{3(s)} \qquad (32)$$

$$Fe^{+2}_{(aq.)} + HCO^{-2}_{3(aq)} \leftrightarrow Fe(HCO_3)_{2\,(s)} \qquad (33)$$

$$Fe(HCO_3)_{2(aq)} \leftrightarrow FeCO_{3(s)} + CO_{2(g)} + H_2O_{(l)} \qquad (34)$$

The formation of $FeCO_3$ through bicarbonate ions was also supported by Davies and Burstein [64], consisting of "multiple-step reactions." They assume that other ions are responsible for the dissolution rate of Fe (reactions
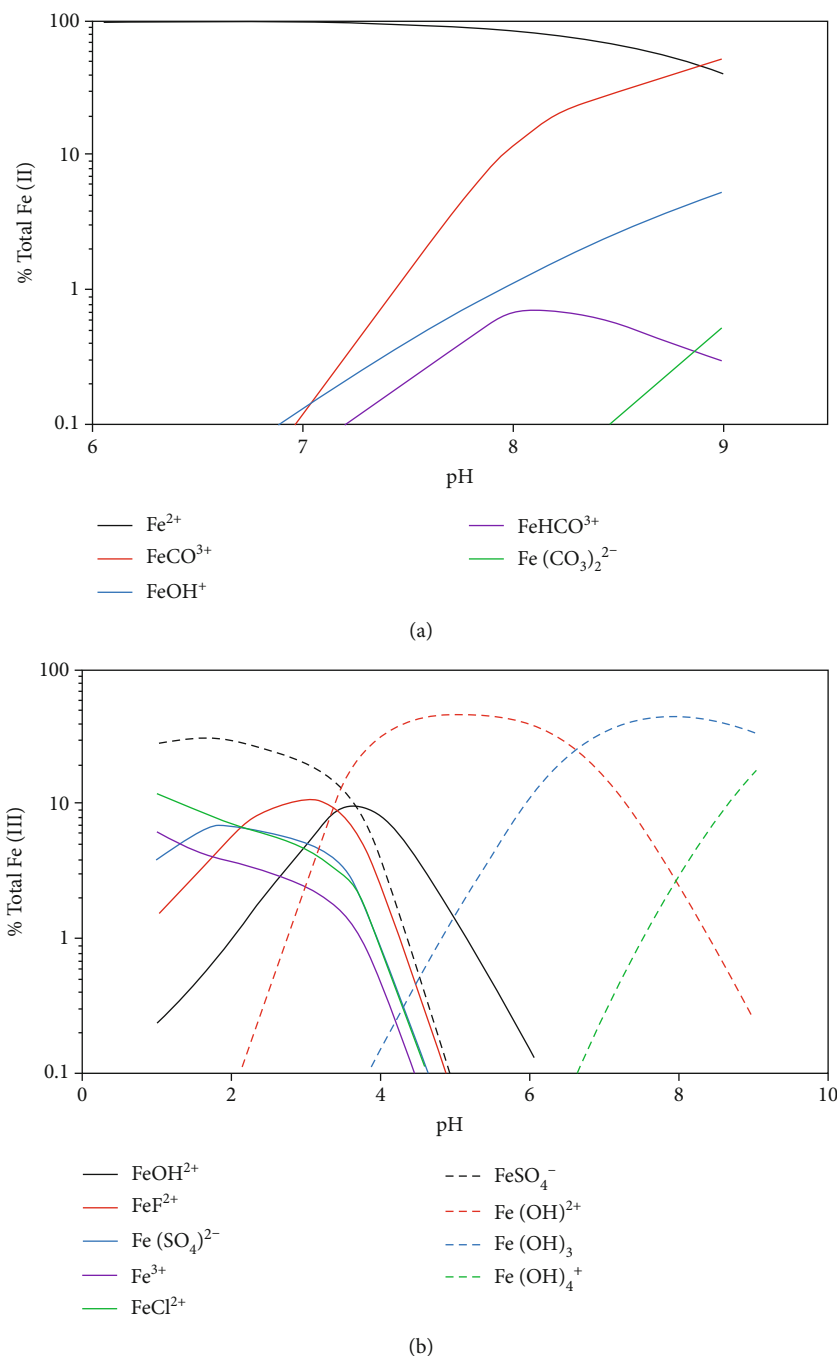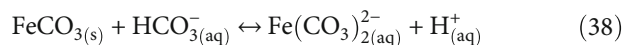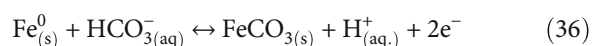
(a)

(b)

FIGURE 3: The speciation of (a) Fe (II) and (b) Fe (III) in seawater according to pH (reproduced from [55] under the Creative Commons Attribution License/public domain).

(35)–(38)). According to the authors, the stable complex anion $Fe(CO_3)_2^{2-}$ should be incorporated into the $CO_{2(g)}$:-Fe:H_2O system, and has a fundamental contribution to pitting formation on the steel surface.

$$Fe_{(s)}^0 + 2H_2O \leftrightarrow Fe(OH)_{2(s)} + 2H_{(aq)}^+ + 2e^- \quad (35)$$

$$Fe_{(s)}^0 + HCO_{3(aq)}^- \leftrightarrow FeCO_{3(s)} + H_{(aq.)}^+ + 2e^- \quad (36)$$

$$Fe(OH)_{2(s)} + HCO_{3(aq.)}^- \leftrightarrow FeCO_{3(s)} + H_2O_{(l)} + OH_{(aq)}^- \quad (37)$$

$$FeCO_{3(s)} + HCO_{3(aq)}^- \leftrightarrow Fe(CO_3)_{2(aq)}^{2-} + H_{(aq)}^+ \quad (38)$$
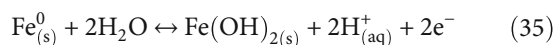
The consensus from the literature is that $FeCO_3$ forms via reactions (24) and (33) [8, 22, 62, 65]. The dissolution of siderite film in acid media should be considered as a sequential reaction.

$$FeCO_{3(S)} + 2H^+_{(aq)} \leftrightarrow Fe^{2+}_{(aq)} + H_2O_{(l)} + CO_{2(aq)} \qquad (39)$$
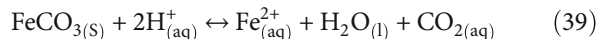
The influence of iron saturation on corrosion rate can be observed in the work carried out by Rogowska et al. [66]. The authors evaluated the influence of the iro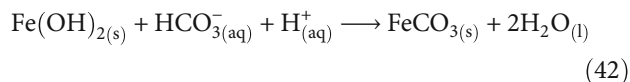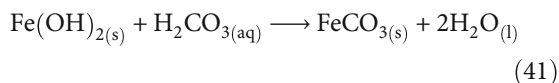n concentration on the corrosion of carbon steel in an environment containing CO_2 at 1 bar. From the mass loss measurements, the general corrosion rates decreased with increasing Fe^{2+} concentration. The addition of 1300 ppm Fe^{2+} resulted in a reduction of 97% in the corrosion rate. On the other hand, without Fe^{2+} in solution, the corrosion rate increases along with 242 h of exposure time. In this sense, the addition of dissolved iron reduces the corrosion rate (Figure 4).

Based on the work of Bockris et al. [27], Linter and Burstein [21] admitted that the presence of a porous scale, formed by $Fe(OH)_2$ before the formation of $FeCO_3$, occurs in a deaerated electrolyte at pH 4. The authors proposed that the CO_2 initial reaction was the formation of $FeCO_3$ from the hydroxide iron layer, resulting in

$$Fe(OH)_{2(s)} + CO_{2(aq)} \longrightarrow FeCO_{3(s)} + H_{2(g)} \qquad (40)$$
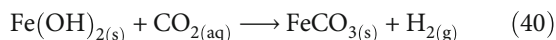
However, gaseous CO_2 can also follow other routes to participate in corrosion reactions through its associated aqueous species. As seen in the research of Kern [67], the dissolved CO_2 in water at pH 4 results in the formation of carbonic acid (H_2CO_3), considered the determinant step for the corrosion mechanism of steel. Afterward, this acid is dissociated into bicarbonate and carbonate ions, respectively, HCO_3^- and CO_3^{2-}. As iron carbonate is stable thermodynamically at pH 4 when compared to iron oxide, according to the Pourbaix diagram, reactions (41) and (42) are expected [29]. In this manner, solid $FeCO_3$ comes from iron hydroxide ($Fe(OH)_2$). Imperfections in the $Fe(OH)_2$ corrosion film, such as pores, allow siderite to grow outside the preexisting hydroxide corrosion scale.

$$Fe(OH)_{2(s)} + H_2CO_{3(aq)} \longrightarrow FeCO_{3(s)} + 2H_2O_{(l)} \qquad (41)$$

$$Fe(OH)_{2(s)} + HCO^-_{3(aq)} + H^+_{(aq)} \longrightarrow FeCO_{3(s)} + 2H_2O_{(l)} \qquad (42)$$

The pH produces a dislocation of equilibria of several species in seawater and modifications to chemical and electrochemical equilibrium. The involved reactions according to the pH range are described below and summarized in Table 3.

(i) For pH lower than 5, a direct reaction of iron with carbonic acid is an alternative route to that proposed by Linter and Burstein [21] in the pH 4. However, $Fe(HCO_3)_{2(s)}$ is unstable and comes to decompose in sequential reactions, creating a solid siderite layer on steel substrate
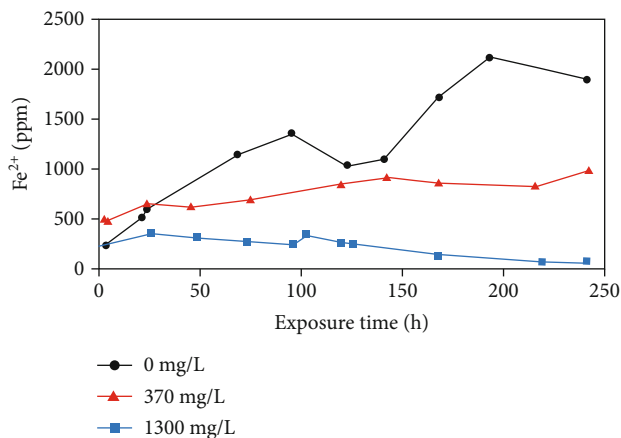

FIGURE 4: Iron dissolved ($Fe^{+2}_{(aq)}$) as a function of time (h) for tests with different initial dissolved iron contents (reproduced from Rogowska et al. [66] under the Creative Commons Attribution License/public domain).

(ii) At pH at around 6.8, some authors predicted that due to a higher concentration of HCO_3^-, direct reduction with iron, and/or iron hydroxide may occur

(iii) For pH higher than 7, the previous reactions comments in reactions become predominant, increasing carbonate and hydroxyl contents in confined seawater. This accumulation of hydroxyl ions (OH^-) in the solution favors the equilibrium related to increasing the concentration of carbonate ions ($CO_3^{2-}_{(aq)}$)

The protection level of hypoeutectic steel is related to the properties of the siderite layer. The conditions of electrolyte supersaturation and impurities in the system influence the scale equilibria at different temperatures and pressures. So, a specific chapter about scale equilibria will be introduced to clarify the topic.

2.2. Scale Equilibria

2.2.1. Supersaturation. The consensus in the literature is that the supersaturation value of siderite (SS) is a critical parameter that provides information about the aggressive or protective character of confined seawater to carbon steel alloy [44, 50, 51]. Barker et al. [4], Burkle [9], Sun et al. [24], Rogowska et al. [66], and several authors represent the SS expression (equation (43)) as the ratio of the product between $Fe^{+2}_{(aq.)}$ and $CO_3^{-2}_{(aq.)}$ by the term K_{sp}.

$$SS_{FeCO_3} = \frac{\left[Fe^{+2}_{(aq)}\right] \cdot \left[CO^{-2}_{3(aq.)}\right]}{k_{sp}}. \qquad (43)$$

Sun et al. [24] reported the modeling of iron saturation considering siderite supersaturation and temperature. The results followed the experiments of Dugstad [68] and originated a unified equation, comprising a better comprehension of the siderite precipitation equilibria. Figure 5 clarifies the situations under saturation and supersaturation

TABLE 3: Reactions and pH range for $CO_{2(g)}$:$H_2O_{(l)}$:steel system [21, 68].

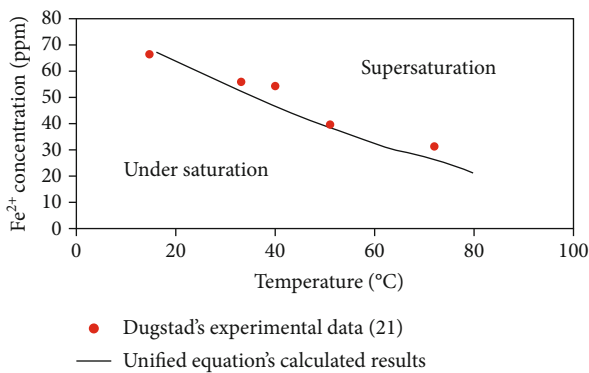| pH	Reactions
Lower than 5 (significant $[H_2CO_3]$)	$Fe_{(s)} + 2H_2CO_{3(aq)} \longrightarrow Fe(HCO_3)_{2(s)} + H_{2(g)}\uparrow$
	$Fe(HCO_3)_{2(s)} \longrightarrow Fe^{2+}_{(aq)} + 2HCO_3^-$
	$HCO^-_{3(aq)} \longrightarrow H^+_{(aq)} + CO^{2-}_{3(aq)}$
	$Fe^{2+}_{(aq)} + CO^{2-}_{3(aq)} \longrightarrow FeCO_{3(s)}$
At 6.8 (significant $[HCO_3^{-2}]$)	$Fe_{(s)} + HCO^{3-}_{(aq)} \longrightarrow FeCO_{3(s)} + H^+_{(aq)} + 2e^-$
	$Fe(OH)_{2(s)} + HCO^-_{3(aq)} \longrightarrow FeCO_{3(S)} + H_2O_{(l)} + OH^-_{(aq)}$
Higher than 7 (significant $[CO_3^{-2}]$)	$Fe^{+2}_{(aq)} + CO^{-2}_{3(aq.)} \leftrightarrow FeCO_{3(s)}$

FIGURE 5: Comparison between the experimental saturated Fe^{+2} concentration provided by Dugstad and the calculated saturated Fe^{+2} concentration using the unified equation at different temperatures (reproduced from Sun et al. [24] under the Creative Commons Attribution License/public domain).

related to iron dissolved and temperature. The similarity between Dugstad's experimental data and the unified equation's calculated results is evident.

Chokshi et al. [69] investigated the effect of different supersaturation values of $FeCO_3$, in a pH range from 6 to 6.6, on the corrosion rates of X65 steel along immersion hours [70]. At pH 6.3, a low level of supersaturation was achieved, $SS = 7$, with the corrosion rate slowly decreasing over time, reflecting the formation of a porous and nonprotective film. However, in the case of pH 6.6, the supersaturation achieved, $SS = 150$, provided a rapid decay of the corrosion rate due to the formation of protective films (Figure 6).
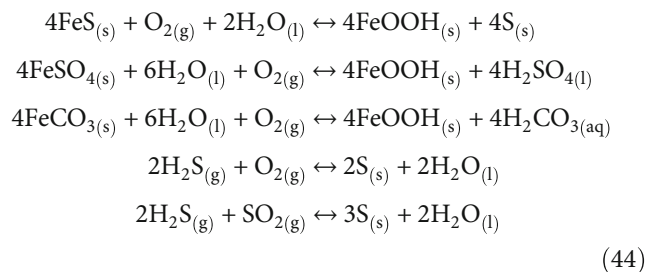
The supersaturation is directly proportional to the $Fe^{+2}_{(aq)}$ concentration (as can be seen in reaction (43)) and, according to De Motte et al. [70], is inversely proportional to the corrosion rate. The authors performed immersion tests at pH 6.3 and 6.8 to investigate the influence of pH on the precipitation of $FeCO_3$ in a brine containing CO_2 at 80°C (Figure 7). At pH 6.8, there is a sharp drop in the corrosion rate over 20 hours of immersion, indicating the formation of a more protective film in comparison to pH 6.3. Additionally, the dissolved iron concentration is much lower in the system with pH 6.8, corroborating the formation of a more protective film at a higher pH value.

De Motte et al. [71] studied the pH developed near the surface of X65 carbon steels during immersion tests. The pH values addressed, pH 6 and pH 6.6, were similar to De Motte et al. [70]. The conditions of the experiments were 80°C and a stagnant solution of pCO_2 at 0.54 bar, with continuous bubbling in brine. The corrosion rates were determined through the linear polarization resistance technique (LPR), and the open circuit potential (OCP) was measured over 12 days of immersion to evaluate the development of a corrosion scale. At the end of the test, corrosion rates of 0.04 and 0.02 mm.y^{-1} were measured for pH 6 and 6.6, respectively. On the other hand, the corrosion rate becomes stable after 9.4 days at pH 6.6 (Figure 8(a)). This behavior agrees with the positive shift potential observed in Figure 8(b), and according to literature [44, 72], this is due to a protective "pseudopassive" film formation, resulting in lower corrosion rates and an increase in OCP values.

Several subsequent publications improved the CO_2:H_2O system studies including the effects of flow rate [73], non-ideal solutions, protective scales [74], and steel microstructures [7].

2.2.2. Scale and Impurities Interactions. $CO_{2(g)}$ impurities transform the corrosion scale formed due to their oxidant properties. Even low quantities of impurities present in $CO_{2(g)}$ are sufficient to generate a galvanic cell after dissolution/recrystallization of siderite film and/or decrease the solubility of water in CO_2, producing more corrosive situations [75–79].

Sun et al. [75] showed that several products present inside a dense phase can interact with the film formed on steel according to the following reactions:

$$4FeS_{(s)} + O_{2(g)} + 2H_2O_{(l)} \leftrightarrow 4FeOOH_{(s)} + 4S_{(s)}$$
$$4FeSO_{4(s)} + 6H_2O_{(l)} + O_{2(g)} \leftrightarrow 4FeOOH_{(s)} + 4H_2SO_{4(l)}$$
$$4FeCO_{3(s)} + 6H_2O_{(l)} + O_{2(g)} \leftrightarrow 4FeOOH_{(s)} + 4H_2CO_{3(aq)}$$
$$2H_2S_{(g)} + O_{2(g)} \leftrightarrow 2S_{(s)} + 2H_2O_{(l)}$$
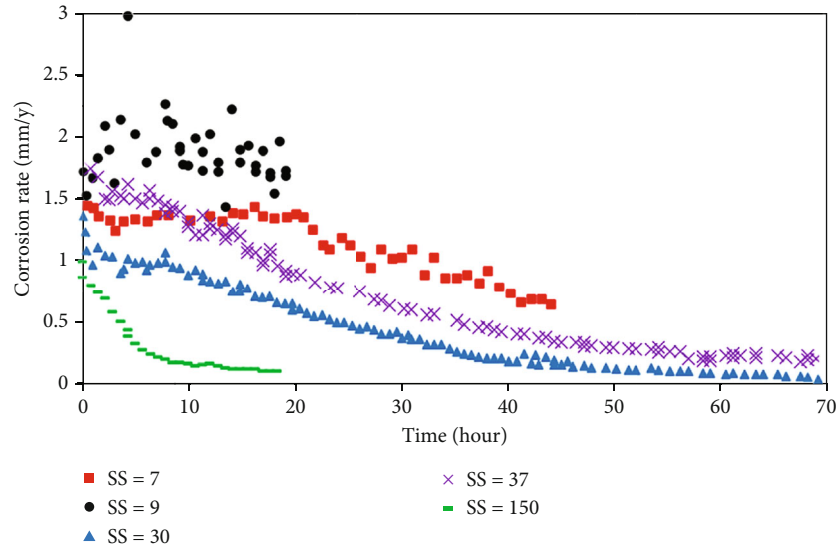$$2H_2S_{(g)} + SO_{2(g)} \leftrightarrow 3S_{(s)} + 2H_2O_{(l)}$$

(44)

FIGURE 6: Effect of supersaturation (SS) on the corrosion rates at $T = 80°C$, no inhibitor, stagnant conditions (provided with permission from the Association of Materials Protection and Performance (AMPP), this is a reproduction of Figure 3 from AMPP C2005-05285, "Iron Carbonate Scale Growth and the Effect of Inhibition in CO_2 Corrosion of Mild Steel," by Kunal Chokshi, Wei Sun, and Srdjan Nesic. Please see the entire document for full context).
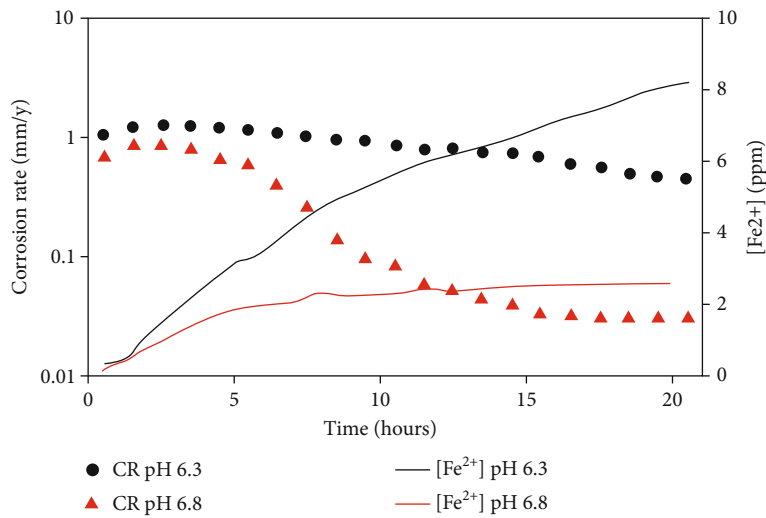

FIGURE 7: Effect of pH on CO_2 corrosion of X65 carbon steel and the resulting cumulative bulk Fe^{2+} ion concentration with time (reproduced from De Motte et al. [70] under the Creative Commons Attribution License/public domain).

The corrosion products can react when in contact with strong oxidants, such as $O_{2(g)}$, and can easily modify the properties of the early corrosion product formed [76, 77]. In comparison, H_2S promotes water-free scales by reducing the $H_2O_{(l)}$ solubility in $CO_{2(g)}$ [78]. The sour corrosion occurs if $H_2S_{(g)}$ pressure exceeds 0.05 times $CO_{2(g)}$ pressure. A mixed process between sour and sweet corrosion occurs only if $H_2S_{(g)}$ pressure is greater than 0.002 times $CO_{2(g)}$ pressure and lower than 0.05 times $CO_{2(g)}$ pressure. So, sour corrosion enhances the corrosion damage to metallic structures [79].

Sun et al. [77] evaluated the stress corrosion of X65 steel at 80 bar of $CO_{2(g)}$ and 50°C in four conditions: (i) 1000 ppm of $O_{2(g)}$, (ii) 1000 ppm of $NO_{2(g)}$, (iii) 1000 ppm of $SO_{2(g)}$, and (iv) 20 grams of $H_2O_{(l)}$. The authors observed that the impurities promoted higher corrosion rates, but NO_2 and SO_2 presented a more pronounced effect than O_2. Additionally, the environments with impurities increased the SCC susceptibility of the steel.

According to Basilico et al. [80], a pseudopassive scale turns steel substrate highly susceptible to localized corrosion by pits, attributed to changes in the local chemistry of corrosion scale, such as dissolution/reprecipitation of siderite and prior precipitation of oxides on the surface alloy by $O_{2(g)}$ contaminants. The authors evidenced a clear tendency to pit formation on API X65 carbon steel immersed in a test
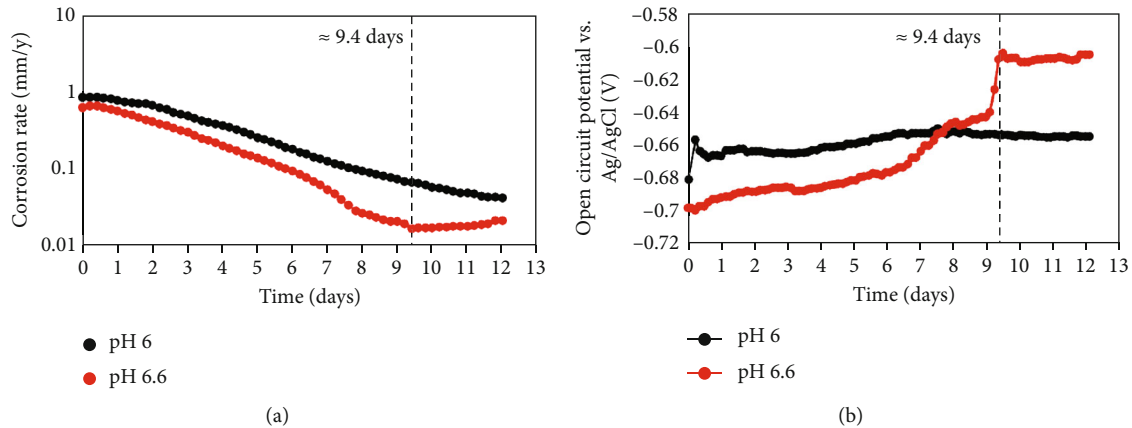
FIGURE 8: Effect of pH on (a) corrosion rate and (b) changing of potential at 80°C, pCO_2 0.54 bar, 0.2 wt% NaCl, and CO_2 saturated solution (reproduced from De Motte et al. [71] under the Creative Commons Attribution License/public domain).

solution with 171 ppb $O_{2(g)}$. The authors attributed a formation of a galvanic pair between O_2-depleted areas (anodic sites) and the rest of the surface (cathodic sites) as the primary mechanism of initiation and propagation of pits, even at very low concentration (hundreds of ppb $O_{2(g)}$). Figure 9 shows the SEM images of the corrosion films obtained during the $O_{2(g)}$ feed, 24 h, and 4 days after the $O_{2(g)}$ feed cut (Figure 9(d)). Chukonavite and magnetite films are achieved in the inner area of the tubercular structures according to Figure 9(a)) under $O_{2(g)}$ contamination. Chukonavite crystals are the main constituent present at pit depth, as evidenced by Figures 9(a) and 9(b), confirming its detrimental effect on the localized corrosion process of carbon steels.

Li et al. [76] employed electrochemical spectroscopy impedance to study the behavior of 5 L X80 steel immersed in a water-rich phase containing CO_2 at 35°C and 80 bar. A similar equivalent circuit composed by $R_e[Q_{dl}[R_T(Q_1R_1)]$ was fitted in the three environments tested: (i) water-rich phase without contaminants, (ii) contaminated by O_2, or (iii) SO_2. The circuit elements can be related to electrolyte resistance (R_e), the constant phase angle element of the electrical double layer (Q_{dl}), charge transfer resistance (R_t), the constant phase angle element related to scale (Q_1), and the resistance related to scale (R_1). The decrease of resistance (R_t and R_1) and increase of constant phase angle element (Q_{dl} and Q_1) values show the deleterious effect of the contaminants compared to the water-rich phase. The presence of $NO_{2(g)}$ as a contaminant shows a circuit composed of $Re[Q_{dl}[R_T(Q_1R_1)W]$. The presence of Warburg impedance (W), the lower resistances (R_T and R_1), and the higher constant phase angle element (Q_{dl} and Q_1) were attributed to the poor adhesion of the scale to the substrate and a gravelly corrosion product.

2.3. Effect of Temperature.
Several studies have been reported on the influence of temperature on corrosion mechanisms for steel alloys [81–86]. The temperature plays a main role in iron carbonate precipitation kinetics, forming a protective or nonprotective film on the steel surface. When the temperature and supersaturation levels in the bulk solution are elevated, significant deposition of corrosion products occurs

and probably leads to the forming of a protective film of siderite ($FeCO_3$) [3]. The precipitation rate is slow, and the relative supersaturation becomes particularly high at low temperatures (<40°C), resulting in a porous and poorly adhered layer, which hinders surface protection [52]. On the other hand, improved steel protection is observed at high temperatures (>60°C) due to the formation of crystalline and dense $FeCO_3$ layers. This is proportionated by the fast precipitation rate of $FeCO_3$ at higher temperatures.

Modeling of siderite precipitation was proposed by Marion et al. [87], following previous studies by Helgeson [88] and Greenberg and Tomson [89]. The equilibrium constant of siderite as a function of temperature can be demonstrated by equations (45)–(47). Thus, the increase in temperature generates a decrease in the solubility product of $FeCO_3$.

$$Log\,k_{sp} = -14.66 + \frac{1365.17}{T_k}, \tag{45}$$

$$Log\,k_{sp} = -59.2385 - 0.041377\,T_k - \frac{-2.1963}{T_k} + 24.5724\,Log\,(T_k), \tag{46}$$

$$Log\,k_{sp} = Log\,k_{298.15} - \frac{\Delta H°}{2.303\,R}\left(\frac{1}{T_K} - \frac{1}{298.15}\right) - \frac{1}{2.303\,RT_k} \\ \times \int_{298.15}^{T_k} \Delta CT_k + \frac{1}{2.303RT_k}\int_{298.15}^{T_K} \Delta Cdln\,T_k. \tag{47}$$

Zhang and Cheng [90] evaluated the corrosion behavior of an API X65 pipeline steel at 30, 60, and 90°C. Electrochemical measurements were conducted in a simulated CO_2-saturated oilfield formation water. The morphology of the corrosion products was characterized by scanning electron microscopy (SEM). The authors observed no scale formation at 30°C, whereas a scale with a compact structure was found at 60 and 90°C. The higher temperature (i.e., 90°C) produced the film with the minimum crystallite size, approximately 1 μm. This was attributed to the increase in
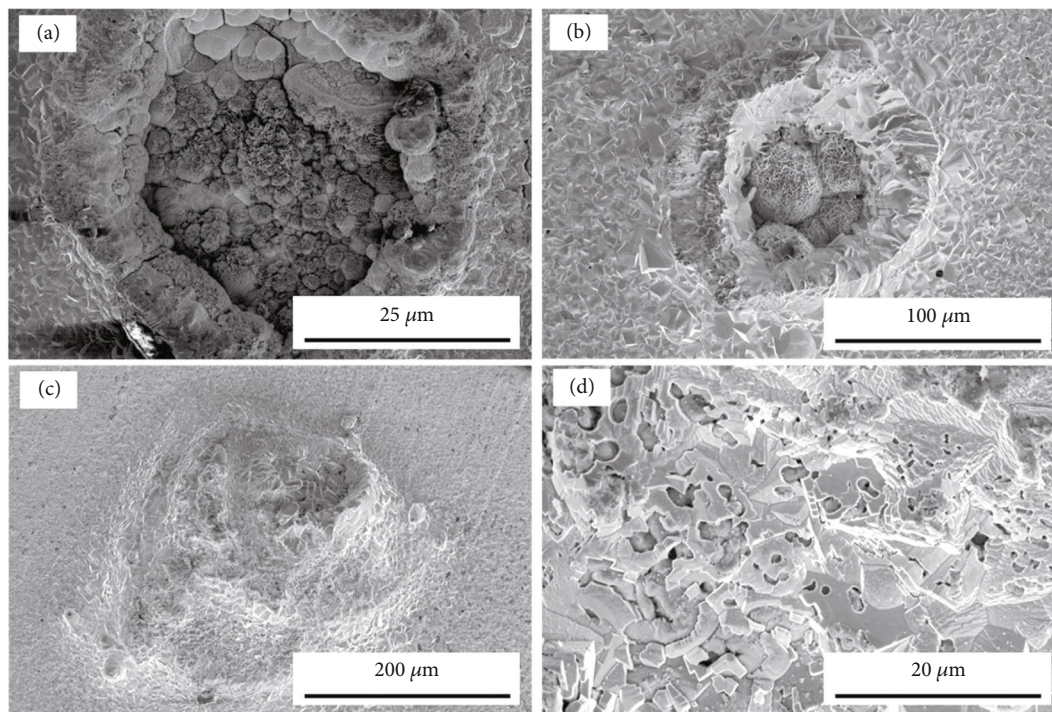
FIGURE 9: SEM images of localized corrosion on API X65 carbon steel (a) during O2(g) feed, (b) 24 h, and (c) 4 days after O2(g) feed cut. (d) Detail of crystals at the base of the pit (reproduced from Basilico et al. [80] under the Creative Commons Attribution License/public domain).

the nucleation rate of $FeCO_3$. Furthermore, substrate protection was enhanced as the temperature increased.

Zhou et al. [91] studied the corrosion film deposited onto Q235 carbon steel at different temperatures. The films formed from 30 to 60°C were poorly compact and adherent, showing some cracks, pores, and gaps. The thickness of the films increased slightly with the increment in temperature. A compact and dense $FeCO_3$ film only began to form at 70°C, and a similar no-crack structure was achieved at 80 and 90°C. The corrosion product achieved at 90°C present crystals coarser and bulkier than those at lower temperatures. In this case, the film was mainly composed of $FeCO_3$ but presented a small amount of Fe_3O_4, which impaired the substrate corrosion resistance and resulted in a higher corrosion rate.

Nešić et al. [42] reported the temperature effect on the precipitation rate/corrosion rate relation of carbon steel immersed in CO_2 solution at 1 bar of CO_2 with pH 6 and dissolved iron concentration at 1 ppm. In tests performed at 50°C, the surface scaling tendency (SST) reached unity and favored the formation of a protective corrosion film. In addition, an increase of a thousand times in precipitation rate kinetic constant (k_{gr}) was observed as the temperature varied from 20 to 70°C. Any protective corrosion product was formed below 50°C because SST < 1 for these conditions.

Experiments were carried out by Honarvar et al. [92] in the temperature range from 55 to 85°C for X70 carbon steel. The samples were immersed in 3 wt% NaCl brine and deaerated with a constant injection of CO_2 at atmospheric pres-

sure. The iron carbonate precipitation was monitored over 72 hours. In the same way as Nešić et al. [42], the minor temperature (i.e., 55°C) was insufficient for iron carbonate formation, independent of the analyzed pH. Honarvar et al. [92] concluded that the iron carbonate precipitation in temperatures below 65°C is not associated with protective properties. On the other hand, the condition at 85°C and pH 6.5 was the better parameter combination for protective iron carbonate formation. The increase in temperature produced a dense and thicker $FeCO_3$ layer.

In order to evaluate the influence of temperature on the corrosive behavior of API X100 steel in solutions containing HCO_3^- and CO_2, Eliyan and Alfantazi [93] varied the concentrations of the bicarbonate ion for the conditions of 20°C and 50°C. The authors calculated the corrosion rates for a solution containing 10 and $50 \, g.L^{-1}$ of bicarbonate. The lower bicarbonate concentration achieved a higher corrosion rate, regardless of the system temperature. Additionally, high bicarbonate levels lead to a higher formation of protective films. The test at 50°C resulted in an abrupt drop in the corrosion rate, evidencing the strong influence of temperature on the kinetics of the corrosion product precipitation from the bicarbonate ion.

Experiments conducted at temperatures above 80°C demonstrated the occurrence of other compounds in the corrosion films besides $FeCO_3$ ([35, 84, 94–96]. Chukanovite ($Fe_2(OH)_2CO_3$) was observed in association with siderite ($FeCO_3$) by Tanupabrungsun et al. [95] in 4-day tests at 80-150°C. $Fe_2(OH)_2CO_3$ is considered a metastable constituent that leads to the formation of $FeCO_3$. The authors

evaluated the morphology of the corrosion products, where prismatic shape crystals were related to siderite presence, whereas plate-like crystals were associated with chukanovite. Regards the corrosion rate, protective films formed above 120°C lead to a decrease in corrosion rate.

Han et al. [94], Hua et al. [84], and De Motte et al. [35] reported the presence of magnetite (Fe_3O_4) between the $FeCO_3$ layer and the steel surface at high temperatures, which generated an improved protective capacity of the substrate by the corrosion films. Han et al. [94] studied the corrosion products formed in X65 steel at 80°C. The tests were conducted in a NaCl solution saturated with CO_2 at pH 8. The results showed the majority formation of $FeCO_3$; however, the elevated local pH created a favorable environment for the formation of Fe_3O_4 near the substrate.

The corrosion behavior of X65 was also evaluated by Hua et al. [84], in the temperature range from 90 to 250°C. The general corrosion rate decreased with increasing temperature, presenting the lowest value (0.36 mm/year) at 200°C. In this condition, the formed film presented gaps between the crystals and reduced coverage. The Raman analysis identified the crystals as FeCO3 and the gap region as Fe_3O_4. Thus, the formation of Fe_3O_4 was more effective in reducing the general and localized corrosion rates on the steel surface compared to cases with only $FeCO_3$ films.

In the work of De Motte et al. [35], the corrosion films obtained at 80°C, 0.54 bar of CO_2, and pH 6.6 also presented Fe_3O_4 in the composition. Figure 10(a)) shows the cross-section analysis of the corrosion film. In the EBSD analysis of the region below the $FeCO_3$ layer (Figure 10(b)), the presence of Fe_3O_4 can be noticed. The formation of magnetite is indicative of a high local pH at the bottom of the pores formed by iron carbonate, which is a close neighbor of magnetite in the stability diagram [94].

It is important to note that during the operation of pipes transporting pressurized fluids, they can be subjected to shut-down operations, where the temperature is low due to gas expansion and pressure drop. The turning condition of the corrosion films is probably different during the component's operational life [97].

2.4. Hydrostatic and CO_2 Partial Pressure Effects. Pressure significantly impacts the solubility of $CO_{2(g)}$ in water, whereas the increase in pressure enhances its dissociation in water and increases carbonic concentrations (H_2CO_3 and HCO_3^{3-}), accelerating the electrochemical reactions and consequently increasing the corrosion rate [82, 98]. Equation (48) [99] shows the relation between corrosion rate and CO_2 partial pressure.

$$\text{Log } V_{corr} = 5.8 - \frac{1710}{T} + 0.67 \text{ Log} \left(p_{CO_2} \right), \quad (48)$$

where V_{corr} is the corrosion rate (mm.y^{-1}), T is the temperature (K), and p_{CO_2} is the CO_2 partial pressure (Pa).

Zhang et al. [33] discussed the corrosion mechanisms of X65 steel at low and high partial pressures of CO_2 (10 and 95 bar, respectively). Different immersion times (from 0.5 to

168 h) were evaluated, and the temperature was kept at 80°C. The corrosion rate decreased rapidly for the first 40 hours of the experiment. After this time, the corrosion rate remained roughly stable for both pressures. It can be noticed that the corrosion rate was much higher for the 95 bar condition (around 28 mm.y^{-1}).

A similar range of pressure (0 to 80 bar) was studied by Suhor et al. [100]. The mild steel exposure to CO_2 for short periods presented a higher corrosion rate at high pressures. On the other hand, the corrosion rate decreased for high pCO_2 (70 and 80 bar) compared to lower pCO_2 values (10, 20, and 40 bar) for longer exposure times. This result was attributed to the passivation effects of the protective layer formed during corrosion assisted by elevated CO_2 pressure, where the $FeCO_3$ layer was able to suppress the corrosion rate to deficient levels (below 0.1 mm.y^{-1}).

The hydrostatic pressure effects in the case of offshore corrosion under higher water depths influence the thermodynamics of the substances, the chemical equilibrium, and, consequently, the electrode reactions. The model proposed by Ma et al. [101] evaluated the influence of hydrostatic pressure on the electrode potential equilibrium and exchange current density and established a corrosion model of metals under deep-sea hydrostatic pressure. According to the authors, the hydrostatic pressure influences the molar volume of materials, affecting their activity and, consequently, the chemical equilibrium.

3. Influence of Hydrodynamic Conditions

Several experimental studies and mathematical models have been reported about the effect of the hydrodynamic conditions on steel's CO_2 corrosion [102–106]. The flow conditions influence the severity of CO_2 corrosion since it impacts the mass transfer process and wall shear stress. Figure 11 illustrates the corrosive process for different flow rates: (a) laminar, (b) transition from laminar to turbulent, and (c) turbulent flow. In the first case (Figure 11(a)), the reduced flow rate allows the formation of a compact and protective layer of $FeCO_3$. On the other hand, increased fluid velocity (laminar/turbulent situation shown in Figure 11(b)) diminishes the diffusion layer thickness formed at the steel surface and results in a porous corrosion film. A higher corrosion rate is observed under these conditions. The extreme case occurs for systems with turbulent flow (Figure 11(c)), where little or no corrosion product is deposited, and the metal is continuously exposed.

In this way, flow parameters impact the $FeCO_3$ precipitation on the steel surface and, consequently, affect the corrosion rates. This occurs because, in the case of turbulent flow, it accelerates the mass transport of corrosive species in the boundary layer adjacent to the metal surface (10–100 μm), turning the metal surface always refreshed with renewed solution and removing any corrosion scale [103, 107]. Among the species involved in sweet corrosion, H^+ presents the highest diffusion coefficient, approximately 9.312 nm^2.s^{-1} (see Table 3). The higher concentration of H^+ results in a more acidic environment, which leads to greater corrosion.
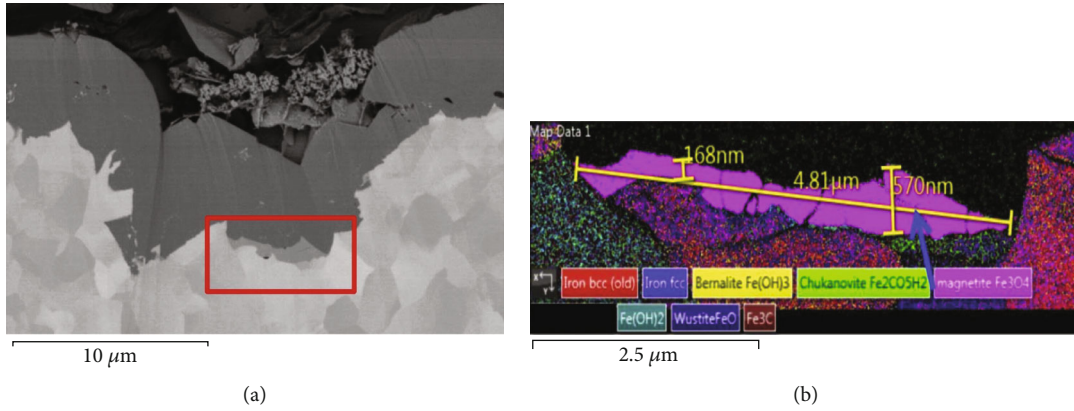
FIGURE 10: (a) Cross-sectional analysis of the corrosion layer formed in API 5 L X65 carbon steel at 80°C, 0.54 bar of CO_2, and pH 6.6. (b) EBSD analysis of the selected region in (a) (reproduced from De Motte et al. [35] under the Creative Commons Attribution License/public domain).
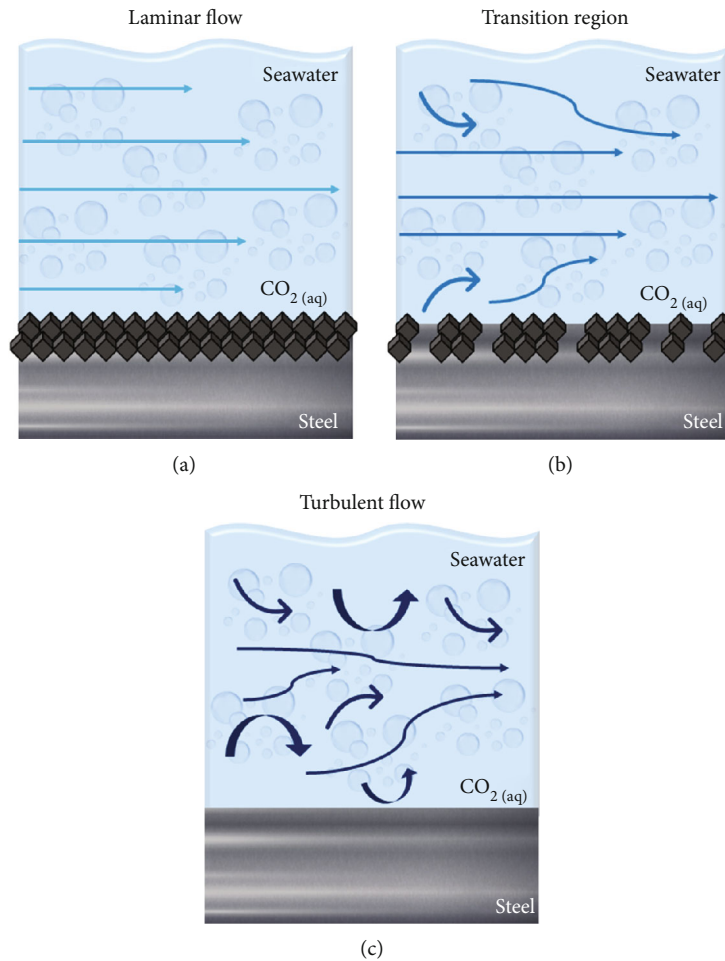
FIGURE 11: Corrosive process representation of (a) laminar, (b) transition from laminar to turbulent, and (c) turbulent flow.

Equation (49) represents a mass transport model covering the boundary conditions from very slow laminar to turbulent flows. This equation results from the contribution of all the transport phenomena involved in CO_2 corrosion: diffusion, migration, convection, and electrochemical reactions on the steel surface (which consume and generate new species) [103]. Table 4 describes the phenomena and their corresponding equation term.

$$\frac{\partial c_i}{\partial t} = -\nabla \left(-D_i \nabla c_i - z_i \frac{D_i}{RT} F c_i \nabla \varphi + c_i u \right) + R, \quad (49)$$

TABLE 4: Equations related to the mass transfer process according to the system region [103].

Region	Transfer process	Equation term
Bulk solution	Diffusion	$-\nabla D\nabla_{C_i}$
	Electromigration	$-Z_i \dfrac{D_i}{RT} F_{C_i}\nabla\varphi$
	Convection	$C_i\mu$
Steel surface	Reactions of precipitation (e.g., $FeCO_{3(ppt)}$)	$-nN_i$

where D_i is the diffusion coefficient of the species i ($m^2 \cdot s^{-1}$), c_i is the concentration of the species i ($mol \cdot m^{-3}$), z_i is the charge number of the species I, F is the Faraday constant (96,500 $C \cdot mol^{-1}$), R is the universal gas constant (8.314 $J\,mol^{-1} \cdot K^{-1}$), T is the temperature (298 K), φ represents the electrostatic potential obtained by solving the electricity model (mV), and u is the electrolyte flow velocity ($m \cdot s^{-1}$).

4. Monitoring, Testing, and Control of Sweet Corrosion

4.1. Monitoring and Testing. The main role in monitoring and assessing the corrosion of equipment and installations in industries is to maintain integrity and reliability, especially in oil and gas, marine, infrastructure, and manufacturing. For that, several methodologies for corrosion parameters monitoring and nondestructive techniques are employed, depending on the objectives, access conditions, and limitations of each technique. This chapter will briefly comment on the characteristics of some of these techniques.

Laboratory tests can be useful to screen materials and parameters for specific conditions and evaluate corrosion rates for strategies of preventive maintenance or inspections. Otherwise, with lab testing results is possible to develop strategies against corrosion, as the use of corrosion inhibitors, protective coatings, or the design of cathodic protection. Another great insight concerning laboratory tests is to evaluate corrosion mechanisms that can occur under specific conditions, once this can be used to implement preventive actions, preventing the occurrence of failures during operation due to an inadequate assessment.

The assessment of the corrosion rate (CR) by mass loss of corrosion coupons is a well-established, widely used, simple, and low-cost technique [108]. In addition, corrosion coupons can be installed in the most diverse environments, allowing visualization of the formed corrosion product. However, this technique has some disadvantages: long periods to get the results, the measurement obtained is an average of the CR only assessing generalized corrosion, and in addition, it can be hazardous to the operator during installation and removal of coupons in service [109]. The standards ASTM-G1 and ASTM-G31 provide guidelines for preparing specimens, test environments, and determining CR using the mass loss method even in the field or in the laboratory.

Nondestructive testing (NDT) complies with noninvasive techniques that provide valuable information regarding material loss due to corrosion and detect cracks or pits resulting from the corrosion process, useful for the asset integrity of most variable structures. The main techniques are based on ultrasonic and electromagnetic techniques and comprise the simplest to sophisticated and complex probes and arrays, based on ultrasonic electromagnetic waves-materials interactions. Guided waves and magnetic flux leakage have been extensively applied as real-time in situ monitoring tools for the inspection of pipelines [110–112]. Both methods are suitable to determine localized and uniform corrosion through the difference in surface thickness. Researchers at LAMEF-UFRGS developed a guided wave ultrasonic collar (array of sensors) to detect corrosion defects in a buried and coated pipeline [112]. The test was conducted for 2 years in a 24 m-long pipeline, with a wall thickness of 9.27 mm and a diameter of 273 mm. Corrosion was induced electrolytically in defects introduced in the coating. The results were satisfactory as the system was able to detect the position (longitudinal and circumferential) of the defects with adequate precision.

Electrochemical tests employed to study the corrosion processes in the laboratory include linear polarization resistance (LPR), potentiodynamic polarization, open circuit potential (OCP), electrochemical impedance spectroscopy, potentiometry, and amperometry [113], as resumed in Table 5.

Electrochemical tests that provide data such as the open circuit potential (OCP) (EN 13509, ISO15589-1) and electrochemical noise (G199-09) are standard methods employed in the oil and gas industry for in situ measurements. LPR is the most employed electrochemical technique due to its fast response, simple operation, and data interpretation. The LPR probes, inserted in the corrosive environment, measure the current flow between electrodes after applying a slight potential (about 10 mV). The linear polarization resistance (ratio of voltage to current) is inversely proportional to the corrosion rate of the material [114]. This technique has been employed in several laboratory investigations [76, 86, 115, 116]. For instance, Eškinja et al. [86] utilized LPR to investigate the corrosion of ferritic steel in a 1.5 wt% NaCl electrolyte under 1 bar CO_2. The authors presented an optimization of the LPR technique by investigating different input values of open circuit potential (OCP) and scan rate. The lowest corrosion rate (1.06 mm.y^{-1}) was measured with a scan rate of 0.05 mV/s. It was observed that lower scan rates produce more accurate results, but the measurements take longer time. Thus, the authors considered 0.125 mV/s as the appropriate scan rate. Moreover, the effect of temperature and time was evaluated to simulate oilfield real conditions and estimate the corrosion of the material in service. The sample tested at the highest temperature (90°C) presented a thick and protective corrosion layer, leading to the lowest corrosion rate.

4.2. Control. As the integrity of the metallic structures in the oil and gas industry is impacted by the harsh operational conditions (for example, high pressure of CO_2 and H_2S),

TABLE 5: Electrochemical techniques commonly used for corrosion monitoring [117, 118].

Electrochemical techniques	Response variable	Application
Electrochemical impedance spectroscopy	Current	Analysis of resistive and capacitive properties of interfaces or surfaces
Electrochemical noise	Potential or current	Detection and quantification of localized corrosion
Linear polarization resistance	Corrosion current	Determination of corrosion rate
Open circuit potential	Potential	Information about activity or passivity of electrode
Chronoamperometry	Current	Charge storage
Chronopotentiometry	Potential	Electrochemical activity
Cyclic voltammetry	Current or potential	Electrochemical activity
Linear polarization	Current or potential	Electrochemical activity and resistance against polarization
Pulse voltammetry	Current or potential	Electrochemical activity

corrosion control is required to avoid or minimize the effects caused by corrosion. Corrosion mitigation methods include material selection and the use of corrosion-resistant alloys, cathodic protection, protective coatings, and corrosion inhibitors, described as follows:

(i) Corrosion-resistant alloys (CRAs) are employed in systems that operate at high pressure and high temperature (HPHT) and in the presence of chlorides, CO_2, and H_2S. Stainless steels and superalloys such as Inconel and Hastelloy, besides titanium alloys, are the most employed CRAs in the industry. They have superior corrosion properties regarding several conditions but are more expensive than carbon steels [119, 120]

(ii) Cathodic protection consists of applying a cathodic corrosion potential to the substrate susceptible to corrosion trough impressed current techniques or sacrificial anodes. The sacrificial anode is a highly active metal (commonly alloys of aluminum, magnesium, or zinc) that corrodes to protect the less active metal of the main structure. DNV recommended practice [121] and NACE/AMPP standard [122] provide guidelines for cathodic protection for offshore applications

(iii) Protective coatings provide a barrier of protection to the metal structures and can be divided into metallic, nonmetallic, and mixed. Metallic coatings have a similar effect to cathodic protection, where a more reactive metal (nickel, zinc, chromium, tin, aluminum, copper, and others) is applied on the steel surface and acts as a sacrificial layer to protect against corrosion. A recent study by Belarbi et al. [123] reported the use of thermal spray aluminum (TSA) coatings to protect gas pipelines from internal CO_2 corrosion. The TSA coating protected the carbon steel surface, and no localized corrosion was observed at 40°C and 4 bar of CO_2. Similarly, a TSA coating was applied by Bertoncello et al. [124] and proved to be effective for suppressing sulfide stress cracking (SSC) and hydrogen-induced

cracking (HIC) of tensile armor steel wires in a sour environment

The application of nonmetallic coatings presents an alternative to substitute metallic coatings. High-performance polymers (HPP) stand out due to their high thermal and chemical resistance and high mechanical strength. They can resist the harsh conditions of the oil and gas industry while maintaining their superior properties. Fluoropolymers, such as Halar® ECTFE (copolymer of ethylene-chlorotrifluoroethylene), have been applied to protect tensile and pressure armor wires of flexible pipes [125]. The polymeric coating exhibited increased resistance to corrosion and its associated failure modes, mainly stress corrosion failures such as stress corrosion cracking induced by CO_2 (SCC-CO_2). Additionally, the coating has proved promising for application in wells with sweet or sour characteristics, high hydrostatic pressures, and in the presence of dense fluids, such as CO_2.

(iv) Inhibitors are chemicals added to the corrosive environments that adsorb on the metal surface and form a protective barrier against corrosion. Literature reports the utilization of inorganic complexes, organic compounds, and natural products as corrosion inhibitors [126–128]. Imidazoline and its derivatives are widely applied to protect pipelines from CO_2 corrosion due to their excellent adsorption on metal surface associated with low toxicity and low cost [129, 130]. Shamsa et al. [131] employed an imidazoline inhibitor composed of tall oil fatty acid (TOFA) and diethylene triamine (DETA) to reduce generalized and localized corrosion of an X65 carbon steel. Different concentrations of inhibitor were studied in a 3 wt% NaCl solution with continuous CO_2 bubbling. The steel samples were significantly corroded without the presence of the inhibitor. In contrast, the essays with ≥30 ppm inhibitor presented surfaces with reduced generalized corrosion. Regarding the localized corrosion, the minor pit depth (1.7 μm) was measured at 40 ppm. So, the results showed that adjusting the inhibitor amount is necessary to minimize both generalized and localized corrosion

5. Concluding Remarks

The corrosion of iron under CO_2 environments has been studied by researchers since 1961. De Waard and Milliams introduced the discussion concerning CO_2 corrosion mechanisms in carbon steels in 1975, which covers mostly the fundamentals of corrosion mechanisms in bulky systems. Although the topic is well-established and published, this review provides the latest data from the available literature on the effects of parameters such as pH, temperature and pressure, hydrodynamics, and the presence of impurities. It was observed that the literature is scarce for confined spaces: systems with supersaturated electrolyte conditions.

The effects of confinement conditions in the flexible pipe annulus are currently being explored. The limited volume where the corrosion takes place, the ionic supersaturation, and the other present constituents could lead to specific effects on the corrosion of carbon steel that are unclear in terms of severity or protectiveness. Considering the current demand of the oil and gas industry, where exploration leads to severe operational conditions, more research and experimental data in confined environments are necessary to better predict the corrosion-related failure modes. Studies on the subject are therefore encouraged.

Conflicts of Interest

The authors declare that they have no conflicts of interest.

Acknowledgments

References

[1] G. Koch, J. Varney, N. Thompson, O. Moghissi, M. Gould, and J. Payer, "Internation measures of prevention, application and economics of corrosion technologies study," (2016). http://impact.nace.org/documents/Nace-International-Report.pdf.

[2] C. De Waard and D. E. Milliams, "Carbonic acid corrosion of steel," Corrosion, vol. 31, no. 5, pp. 177–181, 1975.

[3] S. Nešić, "Key issues related to modelling of internal corrosion of oil and gas pipelines - A review," Corrosion Science, vol. 49, no. 12, pp. 4308–4338, 2007.

[4] R. Barker, D. Burkle, T. Charpentier, H. Thompson, and A. Neville, "A review of iron carbonate ($FeCO_3$) formation in the oil and gas industry," Corrosion Science, vol. 142, pp. 312–341, 2018.

[5] A. Kahyarian, B. Brown, and S. Nesic, "Electrochemistry of CO_2 corrosion of mild steel: Effect of CO_2 on iron dissolution reaction," Corrosion Science, vol. 129, pp. 146–151, 2017.

[6] T. C. Almeida, M. C. E. Bandeira, R. M. Moreira, and O. R. Mattos, "Discussion on "electrochemistry of CO2 corrosion of mild steel: effect of CO2 on iron dissolution reaction" by A. Kahyarian, B. Brown, S. Nesic, [Corros. Sci. 129 (2017) 146–151]," Corrosion Science, vol. 133, pp. 417–422, 2018.

[7] B. Turner and R. Thethi, "Study examines riser system applications, industry trends," Www.Offshore-Mag.Com (n.d.). https://www.offshore-mag.com/subsea/article/16754961/study-examines-riser-system-applications-industry-trends.

[8] Y. Bai and Q. Bai, Subsea Pipelines and Risers, Elsevier, Amsterdam, 1st edition, 2005.

[9] D. P. Burkle, Understanding the formation of protective FeCO3 on to carbon steel pipelines during CO2 corrosion, University of Leeds, 2017.

[10] B. Kermani and D. Harrop, Corrosion and materials in hydrocarbon production: a compendium of operational and engineering aspects, John Wiley & Sons, Ltd, Chichester, UK, 2019.

[11] P. Sui, J. Sun, Y. Hua et al., "Effect of temperature and pressure on corrosion behavior of X65 carbon steel in water-saturated CO_2 transport environments mixed with H_2S," International Journal of Greenhouse Gas Control, vol. 73, pp. 60–69, 2018.

[12] T. C. Almeida and M. C. E. Bandeira, "The effect of high partial pressure of CO2 on the corrosion mechanism of carbon steel in H2O-CO2 systems," Corrosion, vol. 11, 2018.

[13] N. R. Rosli, Y.-S. Choi, and D. Young, "4299: impact of oxygen ingress in CO2 corrosion of mild steel," Corrosion, vol. 15, 2014.

[14] A. V. Afanasyev, A. A. Mel'nikov, S. V. Konovalov, and M. I. Vaskov, "The analysis of the influence of various factors on the development of stress corrosion defects in the main gas pipeline walls in the conditions of the European part of the Russian Federation," International Journal of Corrosion, vol. 2018, Article ID 1258379, 10 pages, 2018.

[15] ANP, "Alerta de Segurança 001 - ANP/SSM: Corrosão sob Tensão por CO2 (SCC-CO2)," (2017). https://www.gov.br/anp/pt-br/assuntos/exploracao-e-producao-de-oleo-e-gas/seguranca-operacional-e-meio-ambiente/incidentes/arquivos-alertas-de-seguranca/alerta-01/alerta-de-seguranca_001_ssm_scc-co2_pt.pdf (accessed June 24, 2020).

[16] J. O. Bockris and D. F. A. Koch, "Comparative rates of the electrolytic evolution of hydrogen and deuterium on iron, tungsten and platinum," The Journal of Physical Chemistry A, vol. 65, pp. 1941–1948, 1961.

[17] W. Lorenz and K. Heusler, Anodic dissolution of iron group metals, Corrosion Mechanisms, 1st edition, 1987.

[18] L. S. Moiseeva and O. V. Kuksina, "On the dependence of steel corrosion in oxygen-free aqueous media on pH and the pressure of CO2," Protection of Metals, vol. 39, pp. 490–498, 2003.

[19] L. G. S. Gray, B. G. Anderson, M. J. Danysh, and P. R. Tremaine, "Effect of pH and temperature on the mechanism of carbon steel corrosion by aqueous carbon dioxide," Corrosion, vol. 40, 1990.

[20] K. S. George and S. Nešić, "Investigation of carbon dioxide corrosion of mild steel in the presence of acetic acid—part 1: basic mechanisms," Corrosion, vol. 63, no. 2, pp. 178–186, 2007.

[21] B. R. Linter and G. T. Burstein, "Reactions of pipeline steels in carbon dioxide solutions," Corrosion Science, vol. 41, no. 1, pp. 117–139, 1999.

[22] J. Hernandez, A. Muñoz, and J. Genesca, "Formation of iron-carbonate scale-layer and corrosion mechanism of API X70

pipeline steel in carbon dioxide-saturated 3% sodium chloride," *Afinidad*, vol. 69, p. 8, 2012.

[23] J. L. Mora-Mendoza and S. Turgoose, "Fe$_3$C influence on the corrosion rate of mild steel in aqueous CO_2 systems under turbulent flow conditions," *Corrosion Science*, vol. 44, no. 6, pp. 1223–1246, 2002.

[24] W. Sun, S. Nešić, and R. C. Woollam, "The effect of temperature and ionic strength on iron carbonate (FeCO$_3$) solubility limit," *Corrosion Science*, vol. 51, no. 6, pp. 1273–1276, 2009.

[25] T. Tran, B. Brown, and S. Nesic, "Corrosion of mild steel in an aqueous CO_2 environment – basic electrochemical mechanisms revisited," *Corrosion*, vol. 11, 2015.

[26] A. Kahyarian, B. Brown, and S. Nesic, "Mechanism of CO2 corrosion of mild steel: a new narrative," *Corrosion*, vol. 16, 2017.

[27] J. O. Bockris, D. Drazic, and A. R. Despic, "The electrode kinetics of the deposition and dissolution of iron," *Electrochimica Acta*, vol. 4, no. 2-4, pp. 325–361, 1961.

[28] G. Cui, Z. Yang, J. Liu, and Z. Li, "A comprehensive review of metal corrosion in a supercritical CO2 environment," *International Journal of Greenhouse Gas Control*, vol. 90, article 102814, 2019.

[29] N. Spycher, K. Pruess, and J. Ennis-King, "CO_2-H$_2$O mixtures in the geological sequestration of CO_2. I. Assessment and calculation of mutual solubilities from 12 to 100˚C and up to 600 bar," *Geochimica et Cosmochimica Acta*, vol. 67, no. 16, pp. 3015–3031, 2003.

[30] M.-C. Caumon, J. Sterpenich, A. Randi, and J. Pironon, "Experimental mutual solubilities of CO2 and H2O in pure water and NaCl solutions," *Energy Procedia*, vol. 114, pp. 4851–4856, 2017.

[31] Y.-S. Choi and S. Nesic, "Corrosion behavior of carbon steel in supercritical CO2 ñ water environments," NACE INTERNATIONAL (2009). https://store.ampp.org/09256-corrosion-behavior-of-carbon-steel-in-supercritical-co2-water-environments (accessed November 21, 2023).

[32] Y.-S. Choi and S. Nešić, "Determining the corrosive potential of CO_2 transport pipeline in high pCO$_2$-water environments," *International Journal of Greenhouse Gas Control*, vol. 5, no. 4, pp. 788–797, 2011.

[33] Y. Zhang, X. Pang, S. Qu, X. Li, and K. Gao, "Discussion of the CO_2 corrosion mechanism between low partial pressure and supercritical condition," *Corrosion Science*, vol. 59, pp. 186–197, 2012.

[34] S. Nesic, J. Postlethwaite, and M. Vrhovac, "CO2 corrosion of carbon steel - from mechanistic to empirical modelling," *Corrosion Reviews*, vol. 15, pp. 211–240, 1997.

[35] R. De Motte, E. Basilico, R. Mingant et al., "A study by electrochemical impedance spectroscopy and surface analysis of corrosion product layers formed during CO_2 corrosion of low alloy steel," *Corrosion Science*, vol. 172, article 108666, 2020.

[36] R. Rizzo, S. Gupta, M. Rogowska, and R. Ambat, "Corrosion of carbon steel under CO2 conditions: effect of CaCO3 precipitation on the stability of the FeCO3 protective layer," *Corrosion Science*, vol. 162, article 108214, 2020.

[37] S. Wang, L. Lamborn, and W. Chen, "Near-neutral pH corrosion and stress corrosion crack initiation of a mill-scaled pipeline steel under the combined effect of oxygen and paint primer," *Corrosion Science*, vol. 187, article 109511, 2021.

[38] Z. Duan and R. Sun, "An improved model calculating CO_2 solubility in pure water and aqueous NaCl solutions from 273 to 533 K and from 0 to 2000 bar," *Chemical Geology*, vol. 193, no. 3-4, pp. 257–271, 2003.

[39] A. Zadeh, I. Kim, and S. Kim, "Charecteristicas of formation and dissociation of CO2 hydrates at different CO2-Water ratios in a bulk condition," *Journal of Petroleum Science and Engineering*, vol. 196, article 108027, 2021.

[40] L. W. Diamond and N. N. Akinfiev, "Solubility of CO2 in water from −1.5 to 100˚C and from 0.1 to 100 MPa: evaluation of literature data and thermodynamic modelling," *Fluid Phase Equilibria*, vol. 208, pp. 265–290, 2003.

[41] M. Pourbaix, "Atlas of electrochemical equilibria in aqueous solutions," *Journal of Electroanalytical Chemistry and Interfacial Electrochemistry*, vol. 13, p. 471, 1967.

[42] S. Nešić, M. Nordsveen, R. Nyborg, and A. Stangeland, "A mechanistic model for carbon dioxide corrosion of mild steel in the presence of protective iron carbonate films—part 2: a numerical experiment," *Corrosion*, vol. 59, pp. 489–497, 2003.

[43] N. Sridhar, "Local corrosion chemistry—a review," *Corrosion*, vol. 73, no. 1, pp. 18–30, 2017.

[44] J. Han, B. N. Brown, D. Young, and S. Nešić, "Mesh-capped probe design for direct pH measurements at an actively corroding metal surface," *Journal of Applied Electrochemistry*, vol. 40, no. 3, pp. 683–690, 2010.

[45] M. Nordsveen, S. Nešić, R. Nyborg, and A. Stangeland, "A mechanistic model for carbon dioxide corrosion of mild steel in the presence of protective iron carbonate films—part 1: theory and verification," *Corrosion*, vol. 59, no. 5, pp. 443–456, 2003.

[46] D. W. Green and M. Z. Southard, *Perry's Chemical Engineers' Handbook*, McGraw Hill Education, New York, 9th edition, 2019.

[47] J. Newman and K. Thomas-Alyea, *Electrochemical Systems*, John Wiley & Sons, Ltd, Canada, 3rd edition, 2004.

[48] J. Kvarekval, "A kinetic model for calculating concentration profiles and fluxes of CO2-related species across the Nernst diffusion layer," in *Nace Corrosion*, Nace, 1997.

[49] D19 Committee, *Practice for the preparation of substitute ocean water*, D19 Committee, 2013.

[50] A. Kahyarian, M. Singer, and S. Nesic, "Modeling of uniform CO2 corrosion of mild steel in gas transportation systems: a review," *Journal of Natural Gas Science and Engineering*, vol. 29, pp. 530–549, 2016.

[51] F. J. Millero, *Chemical Oceanography*, CRC press, 4th edition, 2013.

[52] A. Dugstad, "06111- Fundamental aspects of CO2 metal loss corrosion part I: mechanism," *Corrosion*, vol. 18, 2006.

[53] M. König, J. Vaes, E. Klemm, and D. Pant, "Solvents and supporting electrolytes in the electrocatalytic reduction of CO_2," *iScience*, vol. 19, pp. 135–160, 2019.

[54] P. J. Worsfold, M. C. Lohan, S. J. Ussher, and A. R. Bowie, "Determination of dissolved iron in seawater: a historical review," *Marine Chemistry*, vol. 166, pp. 25–35, 2014.

[55] F. J. Millero, W. Yao, and J. Aicher, "The speciation of Fe(II) and Fe(III) in natural waters," *Marine Chemistry*, vol. 50, no. 1-4, pp. 21–39, 1995.

[56] F. Farelas, M. Galicia, B. Brown, S. Nesic, and H. Castaneda, "Evolution of dissolution processes at the interface of carbon

steel corroding in a CO_2 environment studied by EIS," *Corrosion Science*, vol. 52, no. 2, pp. 509–517, 2010.

[57] T. Tanupabrungsun, "2291: iron carbide and its influence on the formation of protective iron carbonate in CO2 corrosion of mild steel," in *NACE CORROSION*, NACE, 2013.

[58] N. Ochoa, C. Vega, N. Pébère, J. Lacaze, and J. L. Brito, "CO_2 corrosion resistance of carbon steel in relation with microstructure changes," *Materials Chemistry and Physics*, vol. 156, pp. 198–205, 2015.

[59] D. A. López, W. H. Schreiner, S. R. de Sánchez, and S. N. Simison, "The influence of carbon steel microstructure on corrosion layers: an XPS and SEM characterization," *Applied Surface Science*, vol. 207, no. 1-4, pp. 69–85, 2003.

[60] E. Remita, B. Tribollet, E. Sutter et al., "A kinetic model for CO2 corrosion of steel in confined aqueous environments," *Journal of the Electrochemical Society*, vol. 155, p. C41, 2007.

[61] F. Grosjean, R. Mingant, J. Kittel et al., "Corrosion and pH prediction in the annulus of flexible pipes under high pressure of CO2," 2016. https://ifp.hal.science/hal-02464447.

[62] T. das Chagas Almeida, M. C. Bandeira, R. M. Moreira, and O. R. Mattos, "New insights on the role of CO2 in the mechanism of carbon steel corrosion," *Corrosion Science*, vol. 120, pp. 239–250, 2017.

[63] S. Nesic, N. Thevenot, and J. L. Crolet, "Electrochemical properties of iron dissolution in the presence of CO2- basics revisited," in *NACE CORROSION*, pp. 24–29, NACE, 1996.

[64] D. H. Davies and G. T. Burstein, "The effects of bicarbonate on the corrosion and passivation of iron," *Corrosion*, vol. 36, no. 8, pp. 416–422, 1980.

[65] M. M. Islam, T. Pojtanabuntoeng, R. Gubner, and B. Kinsella, "Electrochemical investigation into the dynamic mechanism of CO2 corrosion product film formation on the carbon steel under the water-condensation condition," *Electrochimica Acta*, vol. 390, article 138880, 2021.

[66] M. Rogowska, J. Gudme, A. Rubin, K. Pantleon, and R. Ambat, "Effect of Fe ion concentration on corrosion of carbon steel in CO2environment," *Corrosion Engineering, Science and Technology*, vol. 51, no. 1, pp. 25–36, 2016.

[67] D. M. Kern, "The hydration of carbon dioxide," *Journal of Chemical Education*, vol. 37, no. 1, p. 14, 1960.

[68] A. Dugstad, "The importance of FeCO3 supersaturation on the CO2 corrosion of carbon steels," *Corrosion*, vol. 14, 1992.

[69] K. Chokshi, W. Sun, and S. Nesic, "Iron carbonate scale growth and the effect of inhibition in co2 corrosion of mild steel," *Corrosion*, vol. 23, 2005.

[70] R. A. De Motte, R. Barker, D. Burkle, S. M. Vargas, and A. Neville, "The early stages of FeCO 3 scale formation kinetics in CO 2 corrosion," *Materials Chemistry and Physics*, vol. 216, pp. 102–111, 2018.

[71] R. De Motte, R. Mingant, J. Kittel et al., "Near surface pH measurements in aqueous CO_2 corrosion," *Electrochimica Acta*, vol. 290, pp. 605–615, 2018.

[72] W. Li, B. Brown, D. Young, and S. Nešić, "Investigation of pseudo-passivation of mild steel in CO2 corrosion," *Corrosion*, vol. 70, no. 3, pp. 294–302, 2014.

[73] S. Tebbal and N. Hackerman, "Liquid film thickness and weak acids in the CO_2 pitting of steel," *Corrosion Science*, vol. 34, no. 11, pp. 1787–1792, 1993.

[74] E. J. W. van Hunnik, B. F. M. Pots, and E. L. J. A. Hendriksen, "The formation of protective FeCO2 corrosion product layers in CO2 corrosion," *Corrosion*, vol. 22, 1996.

[75] C. Sun, J. Liu, J. Sun, X. Lin, and Y. Wang, "Probing the initial corrosion behavior of X65 steel in CCUS-EOR environments with impure supercritical CO2 fluids," *Corrosion Science*, vol. 189, article 109585, 2021.

[76] C. Li, Y. Xiang, R. Wang et al., "Exploring the influence of flue gas impurities on the electrochemical corrosion mechanism of X80 steel in a supercritical CO2-saturated aqueous environment," *Corrosion Science*, vol. 211, article 110899, 2023.

[77] C. Sun, X. Yan, J. Sun, J. Pang, W. Zhao, and X. Lin, "Unraveling the effect of O2, NO2 and SO2 impurities on the stress corrosion behavior of X65 steel in water-saturated supercritical CO2 streams," *Corrosion Science*, vol. 209, article 110729, 2022.

[78] C. Sun, J. Sun, and J.-L. Luo, "Unlocking the impurity-induced pipeline corrosion based on phase behavior of impure CO2 streams," *Corrosion Science*, vol. 165, article 108367, 2020.

[79] G. Gabetta, S. Correra, S. Sgorlon, and M. Bestetti, "Test conditions for pipeline materials selection with high pressure sour gas," *International Journal of Corrosion*, vol. 2018, Article ID 3402692, 9 pages, 2018.

[80] E. Basilico, S. Marcelin, R. Mingant et al., "Effect of O2 contamination on carbon steel pseudo-passive scales in CO2 aqueous solutions," *Corrosion Science*, vol. 205, article 110388, 2022.

[81] Z. F. Yin, Y. R. Feng, W. Z. Zhao, Z. Q. Bai, and G. F. Lin, "Effect of temperature on CO 2 corrosion of carbon steel," *Surface and Interface Analysis*, vol. 41, pp. 517–523, 2009.

[82] R. Elgaddafi, A. Naidu, R. Ahmed et al., "Modeling and experimental study of CO2 corrosion on carbon steel at elevated pressure and temperature," *Journal of Natural Gas Science and Engineering*, vol. 27, pp. 1620–1629, 2015.

[83] H. Karimi Abadeh and M. Javidi, "Assessment and influence of temperature, NaCl and H2S on CO2 corrosion behavior of different microstructures of API 5 L X52 carbon steel in aqueous environments," *Journal of Natural Gas Science and Engineering*, vol. 67, pp. 93–107, 2019.

[84] Y. Hua, S. Xu, Y. Wang et al., "The formation of FeCO3 and Fe3O4 on carbon steel and their protective capabilities against CO2 corrosion at elevated temperature and pressure," *Corrosion Science*, vol. 157, pp. 392–405, 2019.

[85] S. Li, Z. Zeng, M. A. Harris, L. J. Sánchez, and H. Cong, "CO2 corrosion of low carbon steel under the joint effects of time-temperature-salt concentration," *Frontiers in Materials*, vol. 6, 2019.

[86] M. Eškinja, M. Moshtaghi, S. Hönig, G. Zehethofer, and G. Mori, "Investigation of the effects of temperature and exposure time on the corrosion behavior of a ferritic steel in CO2 environment using the optimized linear polarization resistance method," *Results in Materials*, vol. 14, article 100282, 2022.

[87] G. M. Marion, D. C. Catling, and J. S. Kargel, "Modeling aqueous ferrous iron chemistry at low temperatures with application to Mars," *Geochimica et Cosmochimica Acta*, vol. 67, pp. 4251–4266, 2003.

[88] H. C. Helgeson, "Thermodynamics of hydrothermal systems at elevated temperatures and pressures," *American Journal of Science*, vol. 267, no. 7, pp. 729–804, 1969.

[89] J. Greenberg and M. Tomson, "Precipitation and dissolution kinetics and equilibria of aqueous ferrous carbonate vs temperature," *Applied Geochemistry*, vol. 7, pp. 185–190, 1992.

[90] G. A. Zhang and Y. F. Cheng, "Localized corrosion of carbon steel in a CO2-saturated oilfield formation water," *Electrochimica Acta*, vol. 56, pp. 1676–1685, 2011.

[91] Y. Zhou, P. Zhang, Y. Zuo, D. Liu, and F. Yan, "The structure and composition of corrosion product film and its relation to corrosion rate for carbon steels in CO2 saturated solutions at different temperatures," *Journal of the Brazilian Chemical Society*, vol. 28, pp. 2490–2499, 2017.

[92] M. Honarvar Nazari, S. R. Allahkaram, and M. B. Kermani, "The effects of temperature and pH on the characteristics of corrosion product in CO2 corrosion of grade X70 steel," *Materials & Design*, vol. 31, pp. 3559–3563, 2010.

[93] F. F. Eliyan and A. Alfantazi, "Influence of temperature on the corrosion behavior of API-X100 pipeline steel in 1-bar CO2-HCO3− solutions: an electrochemical study," *Materials Chemistry and Physics*, vol. 140, pp. 508–515, 2013.

[94] J. Han, D. Young, H. Colijn, A. Tripathi, and S. Nesic, "Chemistry and structure of the passive film on mild steel in CO2 corrosion environments |," *Industrial & Engineering Chemistry Research*, vol. 48, no. 13, 2009.

[95] T. Tanupabrungsun, D. Young, B. Brown, and S. Nesic, *Construction and verification of Pourbaix diagrams for CO 2 corrosion of mild steel valid up to 250°C*, NACE-International Corrosion Conference Series, 2012.

[96] G. R. Joshi, K. Cooper, X. Zhong et al., "Temporal evolution of sweet oilfield corrosion scale: phases, morphologies, habits, and protection," *Corrosion Science*, vol. 142, pp. 110–118, 2018.

[97] D. Fergestad and S. Are Løtveit, *Design and operation of flexible pipes*, DuraSpace, 2017.

[98] M. Mahlobo, K. Premlall, and P. Olubambi, "Effect of CO$_2$ partial pressure and different CO$_2$ phases on carbon steel corrosion," *IOP Conference Series: Materials Science and Engineering*, vol. 272, article 012032, 2017.

[99] H. Bai, Y. Wang, Y. Ma, Q. Zhang, and N. Zhang, "Effect of CO2 partial pressure on the corrosion behavior of J55 carbon steel in 30% crude oil/brine mixture," *Materials*, vol. 11, p. 1765, 2018.

[100] M. F. Suhor, M. F. Mohamed, A. M. Nor, M. Singer, and S. Nesic, "Corrosion of mild steel in high CO 2 environment: effect of the FeCO 3 layer," *NACE-International Corrosion Conference Series*, vol. 5, pp. 3447–3456, 2012.

[101] R. Ma, Y. Shen, C. Wang, J. Dong, and W. Ke, "Effect of hydrostatic pressure on the thermodynamic and kinetic behavior of metal electrode reactions," *Electrochimica Acta*, vol. 424, article 140617, 2022.

[102] X. Chen, X. Yang, M. Zeng, and H. Wang, "Influence of CO2 partial pressure and flow rate on the corrosion behavior of N80 steel in 3.5% NaCl," *International Journal of Electrochemical Science*, vol. 18, article 100218, 2023.

[103] K. Wang, C. Li, Y. Li, J. Lu, Y. Wang, and X. Luo, "A fully coupled model of hydrodynamic-chemical-electrochemical processes for CO2 uniform corrosion in multi-physics environment," *Journal of Petroleum Science and Engineering*, vol. 193, article 107436, 2020.

[104] R. Elgaddafi, R. Ahmed, and S. Shah, "The effect of fluid flow on CO2 corrosion of high-strength API carbon steels," *Journal of Natural Gas Science and Engineering*, vol. 86, article 103739, 2021.

[105] J. Zhao, D. Xiong, Y. Gu, Q. Zeng, and B. Tian, "A comparative study on the corrosion behaviors of X100 steel in simu-
lated oilfield brines under the static and dynamic conditions," *Journal of Petroleum Science and Engineering*, vol. 173, pp. 1109–1120, 2019.

[106] L. R. M. Ferreira, H. A. Ponte, L. S. Sanches, and A. C. T. G. Abrantes, "CO2 Corrosion in the region between the static and turbulent flow regimes," *Materials Research*, vol. 18, pp. 245–249, 2015.

[107] S. Nesic, "Effects of multiphase flow on internal CO $_2$ corrosion of mild steel pipelines," *Energy Fuels*, vol. 26, pp. 4098–4111, 2012.

[108] R. Singh, "Hazards and threats to a pipeline system," in *Pipeline Integrity Handbook*, pp. 35–88, Elsevier, 2017.

[109] R. F. Wright, P. Lu, J. Devkota, F. Lu, M. Ziomek-Moroz, and P. R. Ohodnicki, "Corrosion sensors for structural health monitoring of oil and natural gas infrastructure: a review," *Sensors*, vol. 19, p. 3964, 2019.

[110] Y. Shi, C. Zhang, R. Li, M. Cai, and G. Jia, "Theory and application of magnetic flux leakage pipeline detection," *Sensors*, vol. 15, pp. 31036–31055, 2015.

[111] R. C. Jacques, H. T. H. De Oliveira, R. W. F. Dos Santos, and T. G. R. Clarke, "Design of an EMAT guided wave collar for coated riser inspection," *IEEE Sensors Journal*, vol. 20, pp. 14662–14669, 2020.

[112] R. C. Jacques, H. H. de Oliveira, R. W. F. dos Santos, and T. G. R. Clarke, "Design and in situ validation of a guided wave system for corrosion monitoring in coated buried steel pipes," *Journal of Nondestructive Evaluation*, vol. 38, no. 3, p. 65, 2019.

[113] A. Khan, A. Qurashi, W. Badeghaish, M. N. Noui-Mehidi, and M. A. Aziz, "Frontiers and challenges in electrochemical corrosion monitoring; surface and downhole applications," *Sensors*, vol. 20, p. 6583, 2020.

[114] J. G. Speight, "Corrosion," in *Subsea and Deepwater Oil and Gas Science and Technology*, pp. 213–256, Elsevier, 2015.

[115] S. Karimi, I. Taji, T. Hajilou et al., "Role of cementite morphology on corrosion layer formation of high-strength carbon steels in sweet and sour environments," *Corrosion Science*, vol. 214, article 111031, 2023.

[116] R. Rizzo, S. Baier, M. Rogowska, and R. Ambat, "An electrochemical and X-ray computed tomography investigation of the effect of temperature on CO$_2$ corrosion of 1Cr carbon steel," *Corrosion Science*, vol. 166, article 108471, 2020.

[117] A. J. Bard and L. R. Faulkner, "Electrochemical Methods Fundamentals and Applications," 2022. http://www.nanoer.net/d/img/%E5%B7%B4%E5%BE%B7+%E7%94%B5%E5%8C%96%E5%AD%A6%E6%96%B9%E6%B3%95+%E5%8E%9F%E7%90%86%E4%B8%8E%E5%BA%94%E7%94%A8+2nd+Edition%E8%8B%B1%E6%96%87%E7%89%88+%E9%9D%9E%E6%89%AB%E6%8F%8F557716.pdf (accessed November 22, 2023).

[118] C. M. A. Brett and A. M. O. Brett, *Electrochemistry: Principles, Methods, and Applications*, Oxford University Press, Oxford; New York, 1993.

[119] B. Craig, A. Rowe, M. Warmack, T. E. Doll, C. Stevens, and K. C. Connors, "Guidelines for the selection of corrosion resistant alloys for CCS and CCUS injection wells," *International Journal of Greenhouse Gas Control*, vol. 129, article 103988, 2023.

[120] M. Askari, M. Aliofkhazraei, R. Jafari, P. Hamghalam, and A. Hajizadeh, "Downhole corrosion inhibitors for oil and

gas production – a review," *Applied Surface Science Advances*, vol. 6, article 100128, 2021.

[121] "DNV-RP-B401 Cathodic protection design - DNV," https://www.dnv.com/oilgas/download/dnv-rp-b401-cathodic-protection-design.html (accessed November 21, 2023).

[122] "SP0387-2019 metallurgical and inspection requirements for cast galvanic anodes for offshore applications," AMPP Store. https://store.ampp.org/sp0387-2014 (accessed November 21, 2023).

[123] Z. Belarbi, J. Tylczak, and M. Ziomek-Moroz, "Mitigating CO2 corrosion of natural gas steel pipelines by thermal spray aluminum coatings," *Corrosion*, vol. 78, no. 1, pp. 68–86, 2022.

[124] J. C. B. Bertoncello, L. Simoni, M. R. Tagliari, A. Scheid, M. T. P. Paes, and C. E. F. Kwietniewski, "Effects of thermal spray aluminium coating on SSC and HIC resistance of high strength steel in a sour environment," *Surface and Coatings Technology*, vol. 399, article 126156, 2020.

[125] M. D. R. Tagliari and M. F. Borges, *Duto Flexível*, Processo De Revestimento E Usos De Duto Flexível, 2020.

[126] D. S. Chauhan, M. A. Quraishi, and A. Qurashi, "Recent trends in environmentally sustainable Sweet corrosion inhibitors," *Journal of Molecular Liquids*, vol. 326, article 115117, 2021.

[127] K. Xhanari, Y. Wang, Z. Yang, and M. Finšgar, "A review of recent advances in the inhibition of sweet corrosion," *The Chemical Record*, vol. 21, pp. 1845–1875, 2021.

[128] D. S. Chauhan, M. A. Quraishi, A. A. Sorour, and C. Verma, "A review on corrosion inhibitors for high-pressure supercritical CO2 environment: challenges and opportunities," *Journal of Petroleum Science and Engineering*, vol. 215, article 110695, 2022.

[129] R. A. Jaal, M. C. Ismail, and B. Ariwahjoedi, "A review of CO_2 corrosion inhibition by imidazoline-based inhibitor," *MATEC Web of Conferences*, vol. 13, article 05012, 2014.

[130] Y. Lu, W. Wang, C. Zhang, and J. Zhao, "A novel imidazoline derivative used as an effective corrosion inhibitor for carbon steel in a CO2/H2S environment," *International Journal of Electrochemical Science*, vol. 14, pp. 8579–8594, 2019.

[131] A. Shamsa, R. Barker, Y. Hua, E. Barmatov, T. L. Hughes, and A. Neville, "Performance evaluation of an imidazoline corrosion inhibitor in a CO_2-saturated environment with emphasis on localised corrosion," *Corrosion Science*, vol. 176, article 108916, 2020.